Some physical aspects of laser lithotripsy

van Swol, Christiaan F.P.

Award date:
1990

SOME PHYSICAL ASPECTS OF LASER LITHOTRIPSY

by: Christiaan F.P. van Swol

student at: Eindhoven University of Technology,
Faculty of Physical Engineering.

May 1990

This research was undertaken at the Laser Centre of the Academic Medical Centre in Amsterdam (1989-1990)

Coach at Laser Centre: Dr. Ir. H.J.C.M. Sterenborg

Coach at University: Dr. Ir. C.M. Massen

Supervisor: Prof. Dr. Ir. H.L. Hagedoorn

Samenvatting

In het afgelopen jaar is onderzoek gedaan naar het mechanisme van laserlithotripsy, wat inhoudt het vergruizen van stenen in de galweg en ureter. In de toekomst zal deze techniek misschien ook gebruikt worden voor het vergruizen van speekselstenen. Gepulst laserlicht met een hoge intensiteit wordt ingekoppeld in het ene uiteinde van een glasfiber. Het andere einde van de glasfiber wordt tegen de te vergruizen steen geplaatst. De glasfiber wordt naar de steen geleid door een endoscoop.

Een mechanisme wordt voorgesteld dat de vergruizing als een thermisch proces beschrijft. De steen wordt opgewarmd, steenmateriaal wordt verdampt en een wolk wordt gevormd tussen glasfiber en steen. Moleculen worden geïoniseerd in de dampwolk door de aanhoudende toevoer van laserenergie. Een minimum energie (drempelenergie) nodig voor vergruizing wordt gedefinieerd, die gelijk geacht wordt te zijn aan de minimum energie nodig om geluidsgolven te genereren aan het steenoppervlak, gedurende de laserpuls. Deze drempelenergie is evenredig met de optische absorptiecoëfficiënt van de steen en omgekeerd evenredig met de oppervlakte van het fiberuiteinde dat tegen de steen is geplaatst. Experimenten zijn gedaan met een flitslamp gepompte dye-laser, die pulsen produceert met een duur van 1.5 ms op een golflengte van 504 nm, en met een Ho:YSGG laser, die pulsen van 250 ms produceert met een golflengte van 2.1 mm. De drempelenergie is gemeten voor verschillende gal- en speeksel-stenen en drie verschillende fibers (met een diameter van resp. 200, 400 en 600 mm). De optische absorptiecoëfficiënt van de verschillende stenen is gemeten, gebruik makende van het opto akoestisch effect.

De resultaten van de experimenten ondersteunen het model niet. Een ander model wordt voorgesteld gebaseerd op deze resultaten.

Table of Contents

List of symbols

symbol	name	unit
c_i	specific heat	J kg^{-1} K^{-1}
C_p	specific heat at constant pressure	J kg^{-1} K^{-1}
C_v	specific heat at constant volume	J kg^{-1} K^{-1}
D_s	thermal diffusivity	m^2 s^{-1}
E_i	energy	J
E_{thr}	threshold energy	J
f	frequency	Hz
H_d	latent heat	J $kmol^{-1}$ m^{-3}
I_0	intensity	W m^{-2}
k_i	thermal conductivity	W m^{-1} K^{-1}
l_i	length	m
M_i	microphone signal	V
p	pressure	Pa
P	power	W
r_i	radius	m
R	radius	m
t_i	time	s
T_i	temperature	K
V_i	volume	m^3
γ	$= C_p/C_v$, ratio of specific heats	1
δ_a	optical absorption length of sample	m
δ_g	thermal diffusion length of gas	m
δ_s	thermal diffusion length of sample	m
θ_0	temperature rise	K
μ_a	optical absorption coefficient	m^{-1}
ρ_i	density	kg m^{-3}
τ_i	time constant for thermal diffusion	s

The subscript 'i' specifies the symbol (explained in the text).

1. Introduction

1.1 General

This research has been performed at the Laser Centre of the Academic Medical Centre (AMC) in Amsterdam. The laser centre supports and coordinates the experimental clinical laser treatments in the AMC, and does research in order to develop new treatments.

In medicine treatments using a laser can be classified, on the basis of the physical mechanism by which the therapeutic goal is achieved [1]:

in thermal use (i) laser light is absorbed by the chromophores in the tissue and heat is produced. Once a temperature of about 60 °C is reached denaturation of the proteins of the tissue starts causing tissue coagulation and at 100 °C or more vaporization (ablation) of the tissue occurs. Carbonization starts at a temperature of 400 °C. An application of thermal use of the laser is tissue welding. In this case the increase of temperature is controlled in such way that the parts of the tissue, to be welded, will stick together by the wound that is induced.

In photo chemical use (ii) the energy of the laser light is absorbed by a dye, that has been added to the tissue, which induces a chemical reaction, which leads to destruction of the tissue. Photo dynamical therapy (PDT) of malignant tumour cells is an application of this mechanism: a photo sensitive dye, that has been injected, which is selectively accumulated by tumour cells, is activated by laser light and oxidizes the tumour cells.

In photo mechanical use (iii) pulsed laser light of high intensity is focussed on tissue. A local mechanical shock wave is induced causing the disruption of the tissue in the focus. This mechanism is used to destruct stones in the common bile duct and ureter.

In photo ablation (iv) laser light of a short wavelength (UV) is used. Absorption of the light leads to the destruction of the C-C bonds of the molecular chains of the tissue. It offers the opportunity to remove tissue in a very controlled way, e.g. to reshape the cornea.

For bio stimulation (v) very low power laser light (mostly IR) is used to stimulate biological processes (e.g. the healing of wounds).

One of the new applications of photo mechanical laser treatment, lithotripsy with a pulsed laser, is the subject of the present research.

1.2 Lithotripsy

In general, lithotripsy is the name used for the technique to fragment stones in the human body. These stones (or calculi) can be ureter, gall or salivary stones. A lot of techniques [2] exist for the treatment of stones in the ureter: a non-invasive modality is to use extra corporeal shock wave lithotripsy (ESWL), which makes use of shock waves, which are focussed through the body onto the stone. A semi-invasive technique is endoscopy in the ureter by insertion of ureteroscopes (a widespread skill). Initially the only technique for dealing with a calculus endoscopically was to trap it in a wire basket under vision and then crunch it or manoeuvre it back out of the ureter. Stones which were tightly impacted in the ureter could not be extracted. Modalities for stone fragmentation which can be used via ureteroscopes make ureteroscopy increasingly useful. Delivering laser light with a high power density to the stone, via a fibre in the ureteroscope, is one of these modalities and it has its specific advantages. It is called laser lithotripsy. Recently the sphere of action of endoscopic stone fragmentation was expanded to the biliary system. Here also laser lithotripsy can provide stone fragmentation where other techniques fail. Salivary lithotripsy has not yet been performed in-vivo. Salivary stones are removed in a surgical way, as no endoscopes are available to enter the salivary gland. However such endoscopes are probably available in future and laser lithotripsy may become a technique suitable for fragmenting salivary stones in-situ.

In the urology department, of the academic medical centre (AMC) in Amsterdam, 28 patients have been treated with laser lithotripsy, of which 25 successfully. Also 14 patients with gall stones [2] have been treated at the gastro enterology department, 7 of them successfully; but here it is far more difficult to position the endoscope to the stone than in the urology case. Salivary stones have been treated in-vitro only, after they had been removed surgically. In this research all stones used have been treated in-vitro. In all cases a pulsed dye laser, which delivers 1.5 μs pulses of green light (504 nm) at 10 Hz, has been used.

1.3 The research

The aim of this research was to increase the knowledge of the physical background of laser lithotripsy: investigate the influence of the colour of the

stones on fragmentation, determine threshold values for the initiation of shock waves and find a method to determine the optical absorption coefficient for stones, in-vivo or in-vitro.

In the next chapter laser lithotripsy will be discussed, its performance , observations and a proposal for the mechanism describing it. The samples which are used and a short description of them is given in chapter 3. In chapter 4 the experiments are described; first the measurements to determine the acoustic threshold energy followed by the measurements to determine the optical absorption coefficient of stones. Theory describing the absorption measurements is also derived. The results of the experiments are presented in chapter 5 in the same order as the experiments are described. At last the results of the different experiments are related to each other and the validity of the mechanism is discussed, followed by a proposal for further research. In the appendices the results are displayed as far as they are not displayed in chapter 5 and a description of the microphone, which is used in the measurements, is given.

2. Laser lithotripsy

Laser lithotripsy is a technique for fragmenting stones, as mentioned in the introduction, using a pulsed laser. It can be performed with different kind of lasers, for instance a flash lamp pumped dye laser or a Q-switched Nd:YAG laser. In this report if the mechanism of laser lithotripsy and the observations while practicing it are presented and discussed, it will be about laser lithotripsy with a micro second pulsed laser (504 nm), otherwise it is mentioned that another laser is used (Ho:YSGG laser).

First it is explained how laser lithotripsy is performed in general, second observations are shown and third a theory for the mechanism of it is proposed.

2.1 Performing laser lithotripsy

The output of a pulsed laser is focussed into one end of a fibre, the other end of the fibre is placed in direct contact with the surface of a stone (see figure 2.1). The fibre has a diameter of 200 μm to 600 μm and is made of quartz. In the in-vitro experiments the stone is immersed in water, to simulate the in-vivo situation.

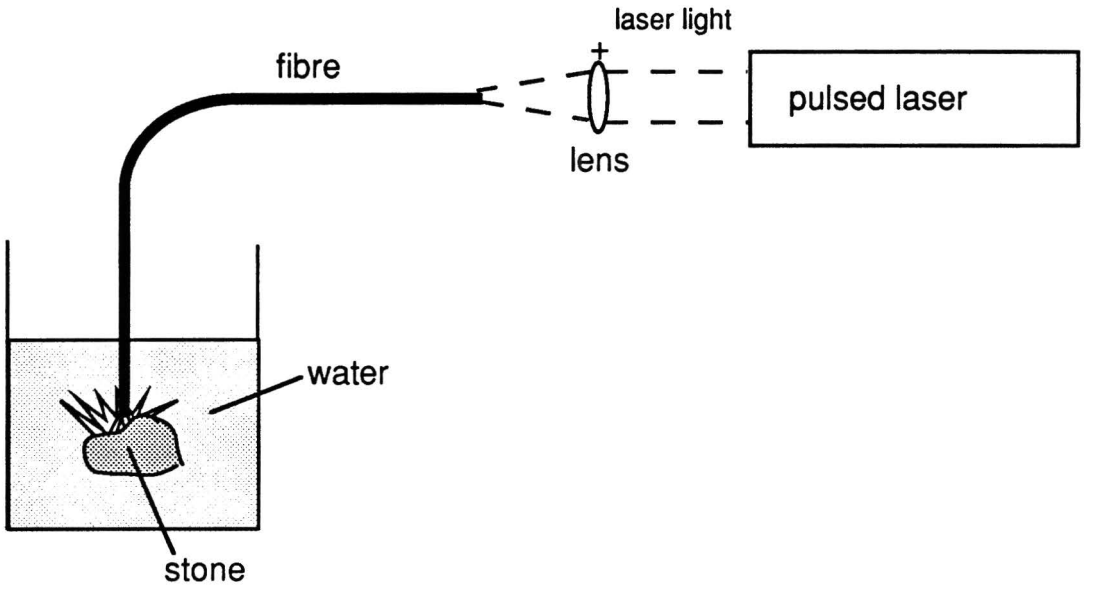

Figure 2.1 Laser lithotripsy.

Depending on the material of the stone and the energy of the pulse a short 'white' flash at the stone surface accompanies the laser pulse, acoustic waves are generated and damage is produced to the stone.

2.2 Description of the mechanism

The light of the laser pulse, delivered with a fibre, is incident on the stone surface. A proposal for the mechanism, which causes damage to the stone, is depicted in figure 2.2.

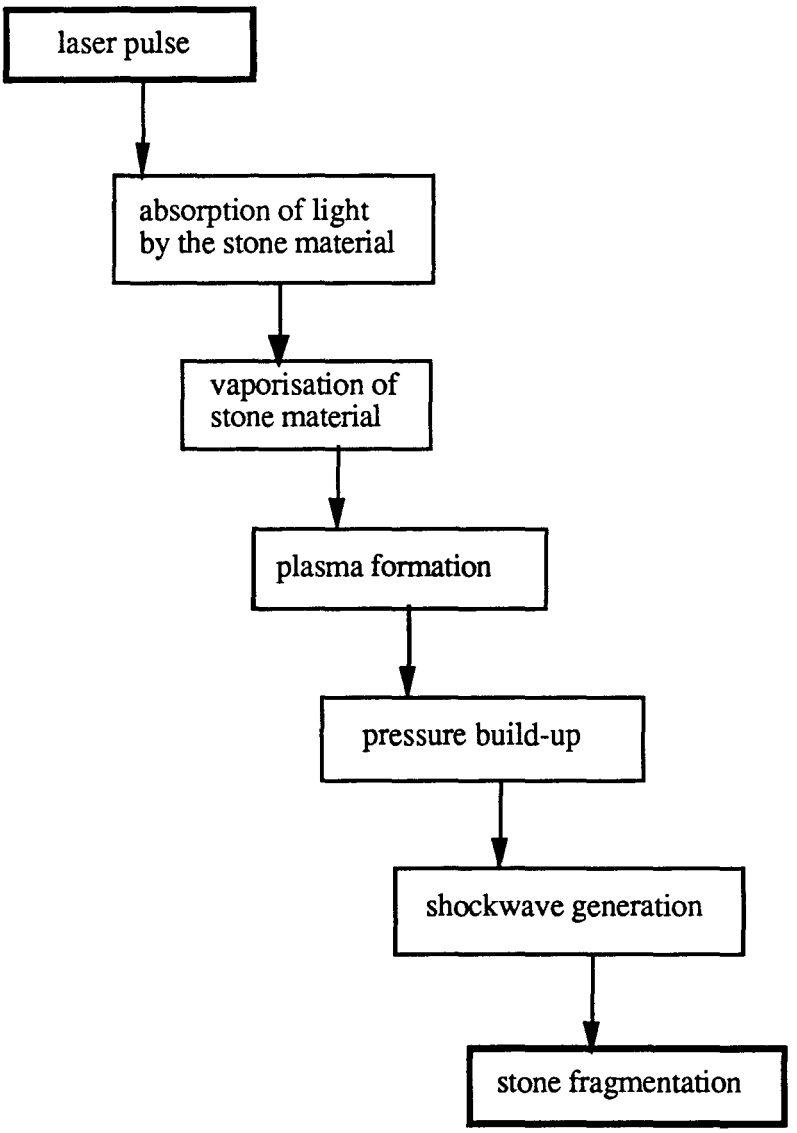

Figure 2.2 The proposed mechanism of laser lithotripsy.

The light produced by the sample during and after one laser pulse, involving the temporal evolution of the emission spectrum, was investigated by Teng et al. [4]. They used a flash lamp pumped dye laser with light pulses of 690 nm and a pulse duration of 0.8 μs (full width at half maximum). Spectra taken very early (0.22 μs) after the beginning of the laser pulse show a continuum (with the shape of the 'Planck'-curve) with absorption lines. After approximately 1 μs these absorption lines disappear and emission lines appear. 'After' 1.60 μs the continuum part of the spectrum disappears and only the emission lines are present. The dominant absorption and emission lines were identified to be Ca II and Ca I. After the laser pulse has ended the plasma disappears and a hot gas bubble remains. As the pressure is very high in this bubble, this bubble expands rapidly. The expansion of the bubble started already with the expansion of the plasma during the laser pulse. After about 500 μs [5] the radius of the bubble reaches a maximum, and the pressure inside reaches a minimum. After that the bubble starts to implode and the radius of the bubble reaches a minimum (and the pressure reaches a maximum). This process of imploding and exploding continues until all energy is lost or the bubble is destroyed. Shock waves are generated, when the pressure build-up in the bubble is high enough. These shock waves are partly absorbed by the stone and produce damage at the surface of the stone or at that place of the stone where the mechanical strength of the stone is small enough.

Looking at the proposed mechanism in figure 2.2 we see that the absorption of light energy is the first in a chain of events. The amount of heat produced due to that absorption depends on (i) the incident power of the laser light, (ii) the light distribution in the stone and (iii) the conduction of the heat produced. The incident power (i) is a function of time: P(t). It is assumed that the light is uniformly distributed (ii) in a cylindrical volume V of which the circular cross section is equal to the fibre cross section (radius of the fibre is r_f) and the length is determined by the optical absorption coefficient of the stone material, μ_a:

$$V = \frac{\pi r_f^2}{\mu_a} \tag{2.1}$$

Van Gemert et al. [6] gives an estimation for the time constant, τ_{diff}, of heat conduction (iii), adapted for a configuration as shown in figure 2.3

$$\frac{1}{\tau_{diff}} = \frac{1}{\tau_z} + \frac{1}{\tau_r} \tag{2.2}$$

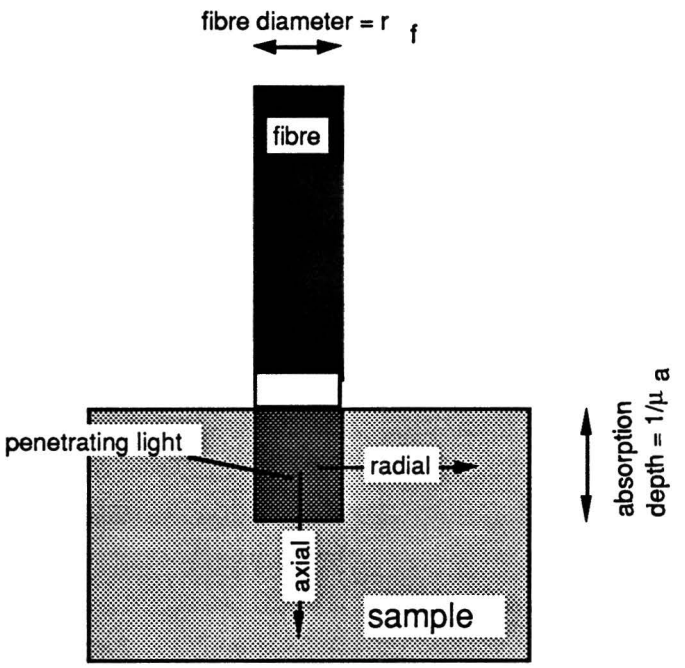

Figure 2.3 Geometry of the thermal diffusion.

with τ_z and τ_r, the time constants for diffusion in the z-direction (axial) and r-direction (radial) respectively:

$$\tau_z = \frac{\rho_s c_s}{k_s}\left(\frac{2}{\pi \mu_a^2}\right) \tag{2.3}$$

and

$$\tau_r = \frac{\rho_s c_s}{k_s}\left(\frac{r_f^2}{2.4}\right) \tag{2.4}$$

where ρ_s, c_s and k_s are the density, the specific heat and the thermal conductivity of the sample material respectively. We use the following

estimations [7] for the (thermal) properties of average stones (granite, sandstone and gypsum),

$$k_s = 1.5 \quad W/mK$$
$$c_s = 800 \quad J/kg\,K$$
$$\rho_s = 1800 \quad kg/m^3$$

and a fibre diameter, r_f, between 200 µm and 600 µm and an absorption coefficient, μ_a, between 2 mm^{-1} and 20 mm^{-1}. The time constants will be in the range:

$$1.5\ ms < \tau_z < 150\ ms$$
$$4.0\ ms < \tau_r < 36\ ms$$

and so τ_{diff} is:

$$1.0\ ms < \tau_{diff} < 30\ ms$$

We can say that as the duration, t_p, of the laser pulse is in the micro second range, the time constant for the process of diffusion τ_{diff} is much shorter than the duration of the pulse and the conduction of heat can be neglected.

The temperature rise, $\partial T(t)$, of the volume V in a time ∂t, due to the absorption of the laser light is related to the power, P(t), of the laser:

$$\rho_s V c_s \frac{\partial T(t)}{\partial t} = P(t) \tag{2.5}$$

where ρ_s is the density of the stone and c_s is the specific heat of the stone. Using equation (2.1) gives:

$$\rho_s \frac{\pi r_f^2}{\mu_a} c_s \frac{\partial T(t)}{\partial t} = P(t) \tag{2.6}$$

Rearranging and integrating this equation yields:

$$T(t) = \frac{\mu_a}{c_s \rho_s \pi r_f^2} \int_0^t P(t)\,dt + T_0 \tag{2.7}$$

where T_0 is the ambient temperature; μ_a, ρ_s and c_s are assumed to be independent of temperature. Let us assume that heating continues until a temperature T_c is reached; T_c being the temperature at which the sample material will vaporize, or dissociate. T_c is reached after a time t_c, which should be shorter than the duration (t_p) of the laser pulse: $t_c < t_p$. If we take the stone properties to be independent of the type of stone, then the heating process only depends on r_f and μ_a (and P(t)). The next step is the dissociation of that part of the stone, which has a temperature T_c. The dissociated material forms a cloud between the fibre end and the surface of the stone. Energy is delivered to the surface and more material is heated and dissociated. Once the cloud of dissociated material is dense enough the temperature of it increases dramatically, by absorption of laser light. Molecules will be ionized: a thermal plasma is formed. The process continues with the, already mentioned, formation of a bubble and shock waves, which leads to the destruction of the stone.

In conclusion we can say that, if the plasma is of main importance for the fragmentation process, the mechanism for plasma initiation is important. As described above, with the assumptions mentioned and a given laser power P(t), the energy needed to create a plasma only depends on fibre diameter and the optical absorption coefficient of the sample. We call this minimum energy the 'plasma threshold energy'. Experiments will be carried out to verify this relation.

3. Samples

For experimental purposes it is better to have reproducible samples, made of a phantom material, instead of real stones obtained from patients, as these stones vary strongly from one another. Phantom materials have been made and they are described in 3.2, first a description of the different stones is given.

3.1 Urinary, gall and salivary stones

The colour of urinary stones [8] varies from white to dark brown. The white stones are mainly made of calcium oxalate dihydrate or a combination with calcium phosphate. The dark stones consist of calcium oxalate monohydrate. Urinary stones with magnesium instead of calcium also exist, but they do not appear often.

Two groups of gall stones [9] can be distinguished, viz. pigment stones and cholesterol stones. Each type contains about 25 % calcium carbonate. Pigment stones are dark brown to black in colour. Their colour comes from bile pigments which are incorporated into the stone as the stone is formed. Cholesterol stones are yellow to white in colour.

The most frequently observed compound of salivary stones [9] is hydroxy apatite, also with traces of magnesium substituted whitlockite. The colour of these stones is white to yellow.

3.2 Phantom stones.

As shown above all stones are based on molecular structures containing calcium. The main compound of salivary stones, i.e. hydroxy apatite, is available as a powder. Adding glue or making tablets, under high pressure, is a possibility to make a solid sample of it. Unfortunately adding glue is not controllable; making tablets of it does work but the result is not satisfying: the tablets 'explode' when they are immersed in water, as the tablet is very hygroscopic. We could not find another way to let it react to obtain a solid sample.

Gypsum is another material that has similarities with stones. It consists merely of calcium sulfate. The process of making it has good reproducibility and it has the advantage that it is easy to add a dye, which makes the optical

absorption coefficient controllable. Samples with different amounts of E110, a food dye, have been made, for use in the experiments.

4. Experiments

Experiments are performed to find out whether the proposed mechanism describes the process of plasma formation. Experiments for obtaining the threshold energy for plasma initiation and for obtaining the absorption coefficient for different samples are carried out. For both experiments the experimental set-up is described, for the absorption measurements also a theory is presented.

4.1 Acoustic threshold measurements

4.1.1 Methods

The acoustic pressure wave coming from a sample during pulsed laser irradiation is detected with a microphone. If the acoustic pressure wave is described by a function of time, p(t), then the microphone signal M(t) is proportional to it:

$$M(t) \propto p(t) \tag{4.1}$$

Equation (4.1) is true when the frequency response of the microphone used is sufficiently flat. The energy of the acoustic wave is proportional to the square of the pressure. The total energy, the wave contains, is E_m:

$$E_m \propto \int_{t=0}^{t=t_e} (M(t))^2 \, dt \tag{4.2}$$

where t=0 is the start of the laser pulse, t_e is the time after which the acoustic wave has become extinct. For energies higher than the plasma threshold energy it is assumed that the relation between the energy of the acoustic pressure wave and the energy of the laser pulse can be approximated with a linear function (figure 4.1):

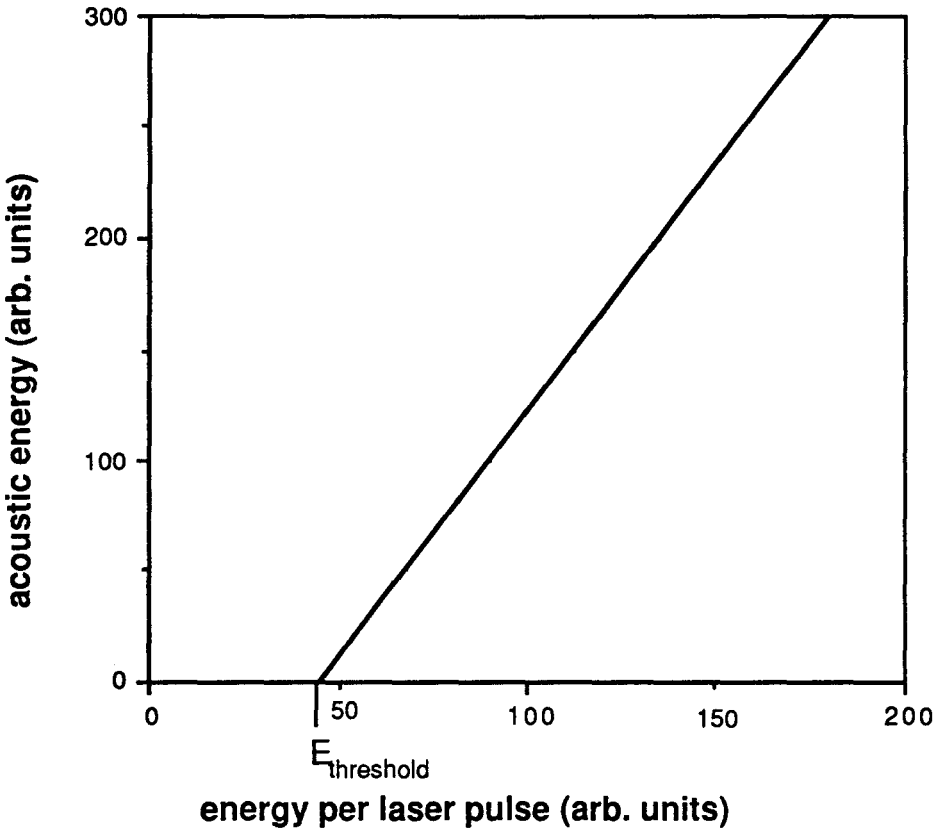

Figure 4.1 Plot of the acoustic energy as a function of laser energy;

The interception with the horizontal axis yields the minimal laser energy needed to generate acoustic waves. This energy is called the acoustic threshold energy, E_{thr}. As plasma formation is assumed to be an essential step leading to shock wave formation, the plasma threshold energy is assumed to be equal to the acoustic threshold energy.

For practical reasons, explained in the next chapter, this way of defining the acoustic threshold energy did not seem to be suitable for stones. A different way was used to define the threshold energy: when looking at the microphone signal on the oscilloscope, only noise is visible when the laser energy is too small to generate a plasma. While increasing the laser energy, the microphone signal will increase suddenly and a 'white' flash is seen. Now the acoustic threshold energy is defined as that amount of energy needed to produce a microphone signal with an amplitude twice as big as the average noise

amplitude. It is assumed that these two definitions lead to the same value of $E_{thr.}$

4.1.2 Apparatus for threshold measurements

The apparatus, used in both experiments and the set-up are presented in figure 4.2:

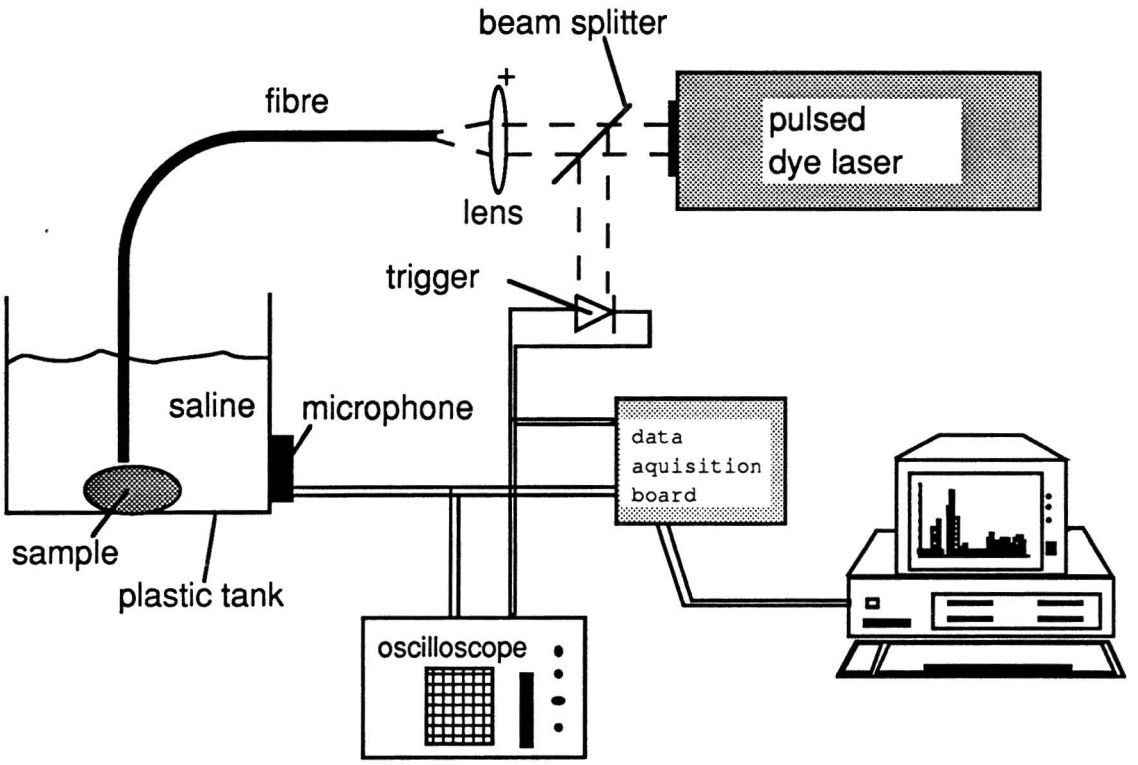

Figure 4.2 Experimental set-up threshold experiments

The laser is a flash lamp pumped dye laser (Candela type LFDL-1). Light with a wavelength of 504 nm is produced by using the dye Coumarine. The duration of the pulse, t_p, is 1.5 μs (full width at half maximum). The repetition rate can be chosen between 1 Hz and 20 Hz. The light is coupled into a fibre which delivers the pulsed light to the surface of the sample. The maximum output energy per pulse is approximately 300 mJ at the laser side and 200 mJ at the far end of the fibre. The sample is a stone or a phantom, made of gypsum with an optical

absorber added. The samples are placed on the bottom of a plastic tank with sizes 10*10*5 cm (L*W*H). The tank is filled with saline in order to approximate the in-vivo situation. The acoustic signal produced at the sample is detected with a crystal microphone, which is fixed at the outside of the tank. The electric signal of the microphone is transmitted to a computer and digitized with a data acquisition board (Keithley series 500, sample rate 40 kHz), and stored. A computer program has been written, to perform this, in 'soft 500', the programming language [10] belonging to the data acquisition board (DAB). Neither the frequency range of the crystal detector nor the sampling rate of the DAB (40 kHz, Δt = 25 μs) is high enough to detect the shock waves. In the first experiments the a.c. part of the stored microphone signal is squared and integrated numerically. In the later experiments only the oscilloscope is used, as the only thing that has to be examined in that case is whether the peak amplitude of the a.c. part of the microphone signal exceeds a certain threshold value. Both oscilloscope and DAB are triggered electronically by the laser pulse.

Apart from the experiment described with the pulsed dye laser the experiment is also performed with a Ho:YSGG laser, with a longer pulse duration (t_p) and with a wavelength, at which the samples have a higher absorption. It should be noted that the time constant for heat diffusion (chapter 2.3) is still long compared with t_p. The pulsed Ho:YSGG laser, which produces pulses with t_p=250 μs at a wavelength of 2.1 μm, is suitable.

4.2 Absorption measurement

In this chapter a method is presented to determine the absorption coefficient of stones using of the photo acoustic effect. In general when light falls on a sample, is absorbed, and sound is generated this effect is called the Opto- or Photo-Acoustics (PA) effect [11]. As there is a wide variety of methods to obtain experimentally the absorption coefficient of samples using this effect, the derivation of the theory below is limited to the method used presently. First this theory is derived, then the experimental set-up is shown and explained.

4.2.1 Theory of the photo acoustic effect

In figure 4.3 a simplified scheme [12] of the experimental apparatus arrangement for a photo acoustic measurement is shown. Light from a continuous wave laser passes through a light chopper to obtain a modulated

light beam. By means of a lens this beam is focussed into a gas container, or on a solid sample in the gas container. Here the intensity of the laser light is chosen so little that no damage is produced to the sample. The acoustic signal, generated in the container, is detected with a microphone and is amplified.

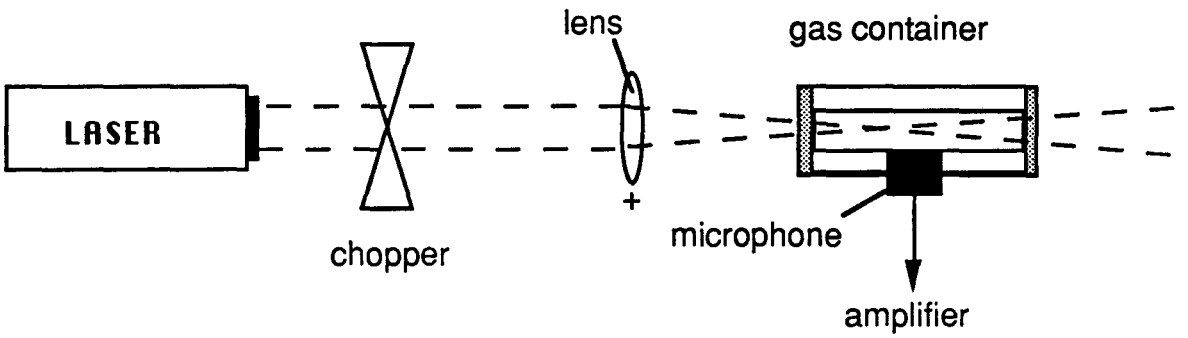

Figure 4.3 Simplified scheme of experimental set-up for the photo acoustic measurement.

In figure 4.4 the stages of the process of the photo acoustic effect are shown.

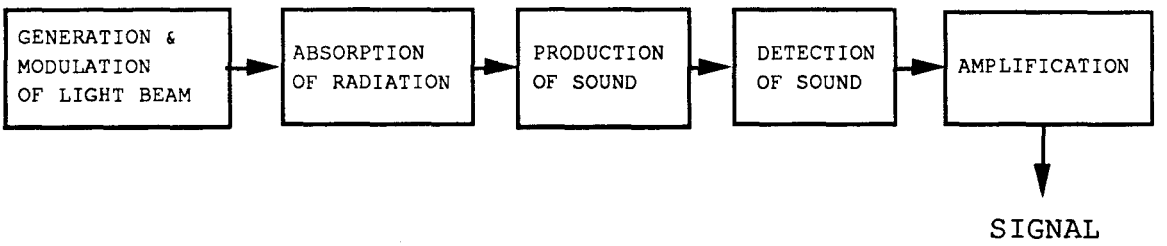

Figure 4.4 Generation of the photo acoustic signal.

Light is incident on a sample that heats up and generates sound. The sound generated, containing information about the sample, is detected and amplified. When investigating solid samples in this way the sample is placed in a gas filled container: the photo acoustic cell (PA-cell). A schematic presentation of a

PA-cell [13,14] is shown in figure 4.5. The cell, which will be used in the experiment is based upon this cell.

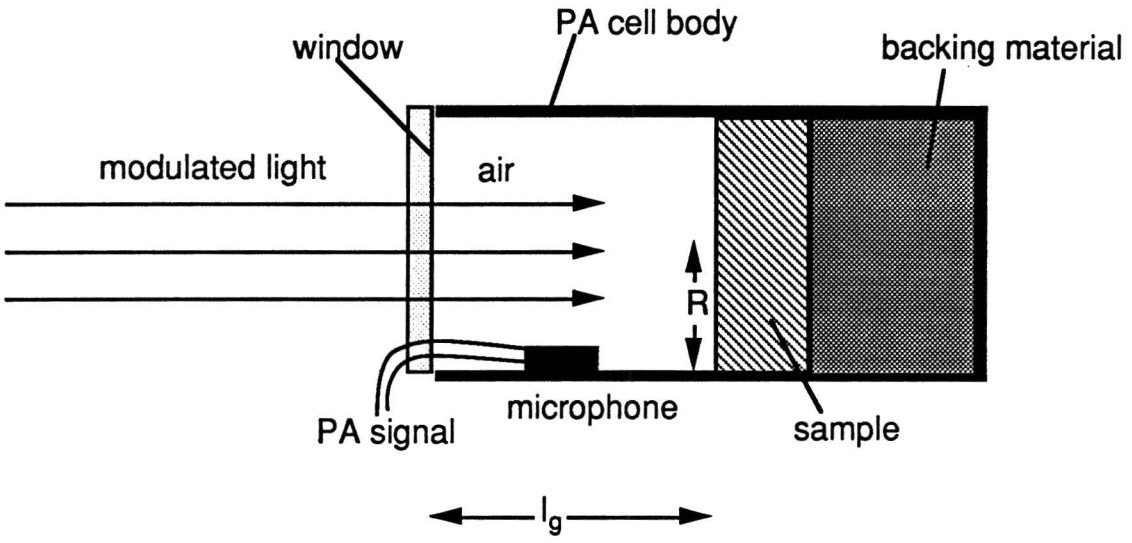

Figure 4.5 General design of a photo acoustic cell

The cell is a cylinder with radius R and filled with air. The walls of the cell are made of thermally isolating material. The length of the gas column is l_g. Deriving the theory it is assumed that the radius of the sample is equal to the radius of the cell. The optical and thermal parameters of the sample should be restricted by:

$$\delta_s < \delta_a < l_s \quad \text{or} \quad \delta_s < l_s < d_a \tag{4.3}$$

where l_s is the length of the sample; δ_a is the optical absorption length of the sample at the exciting wavelength, which is the reciprocal of the optical absorption coefficient μ_a: $\delta_a = 1/\mu_a$; δ_s is the thermal diffusion length of the sample, which depends on the thermal conductivity k_s, the specific heat c_s, the density ρ_s and the frequency f of the modulated light [15]:

$$\delta_s = \sqrt{\frac{k_s}{c_s \rho_s \pi f}} \tag{4.4}$$

By introducing the thermal diffusivity D_s,

$$D_s = \frac{k_s}{c_s \rho_s} \tag{4.5}$$

(4.4) becomes:

$$\delta_s = \sqrt{\frac{D_s}{\pi f}} \tag{4.6}$$

The geometry, belonging with equation 4.3, has been drawn below:

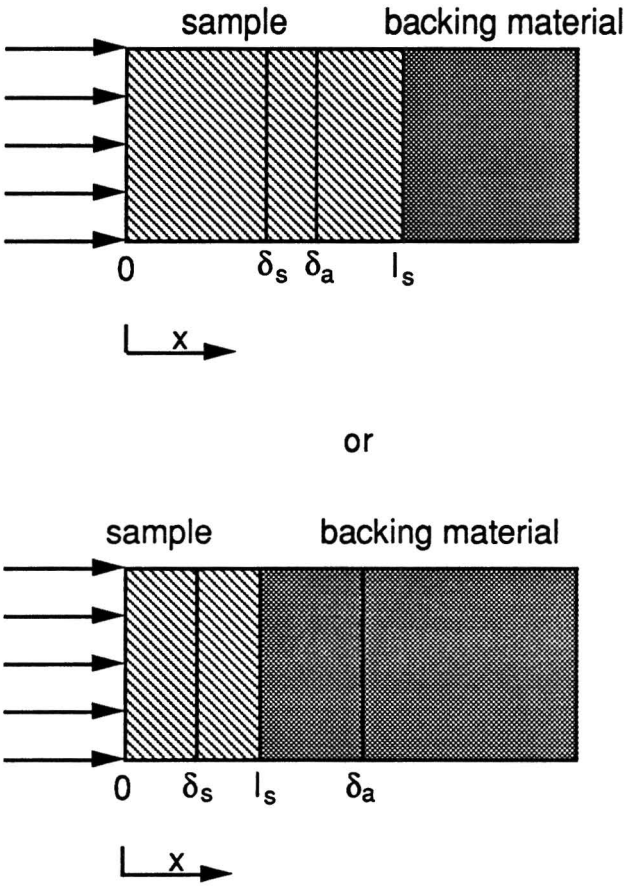

Figure 4.6 Two possible geometries for δ_a, δ_s and l_s of the samples.

The heat, because of radiation of the sample, which really causes the increase of temperature at the surface, only comes from a layer with thickness δ_s, the thermal diffusion length. If the modulated light has an intensity I_0, then the equation for the conduction of heat, in case of a geometry of the properties of the sample δ_a, δ_s and l_s, as drawn in figure 4.6, can be approached by:

$$k_s \left(\frac{\theta_0}{\delta_s} \right) \approx I_0 \left(\frac{\delta_s}{\delta_a} \right) \tag{4.7}$$

as the heat produced in a layer of thickness δ_s is only a fraction δ_s/d_a of the power input of the light that is being absorbed in a layer of thickness δ_a. Here θ_0

is the amplitude of the temperature change at the surface, thus θ_0/δ_s is an estimate for the temperature gradient. θ_0 becomes

$$\theta_0 \approx I_0 \frac{\mu_a \delta_s^2}{k_s} \tag{4.8}$$

The periodic heat diffusion, that will occur, causes temperature variations in that part of the gas which is thermally coupled to the sample. For this part a layer with thickness δ_g, one thermal diffusion length of the gas (air) is taken. This layer will act as a piston: its volume increases, because it is heated up, and it pushes the rest of the gas in the cell, in which way sound is generated. According to figure 4.5 the volume, V_{act}, of this layer, the piston, is:

$$V_{act} = \pi R^2 \delta_g \tag{4.9}$$

δ_g should be smaller than the length of the air column, l_g. According to the Boyle-Gay-Lussac law for ideal gasses, a change in temperature θ_0 gives a change in volume ΔV:

$$\Delta V = \frac{\theta_0}{T} V_{act} \tag{4.10}$$

where T is the absolute temperature. The volume change of this gas piston causes a pressure change in the cell. Assuming that this process is adiabatic,

$$P V^{\gamma} = \text{constant} \tag{4.11}$$

with

$$\gamma = \frac{C_p}{C_v} \tag{4.12}$$

This together with equation (4.10) gives an expression for the amplitude of the pressure change Δp relative to the absolute pressure p:

$$\Delta p = \frac{\Delta V}{V_0} \gamma p \tag{4.13}$$

For V_0, the total volume of air in the cell, we write:

$$V_0 = \pi R^2 l_g \tag{4.14}$$

Combining equations (4.8),(4.9),(4.10),(4.13) and (4.14) an expression for the Δp in the PA-cell, due to the PA-effect, is obtained:

$$\Delta p = \frac{\gamma p \delta_g l_0}{T l_g} \frac{\mu_a \delta_s^2}{k_s} \tag{4.15}$$

This expression shows that in this model Δp is proportional to the optical absorption coefficient μ_a of the sample, when assumptions, as mentioned above are made.

4.2.2 Design of the photo acoustic cell

The design of the PA-cell did change before ending up with the design as it is now. The first cell, that has been made, is shown in figure 4.7.

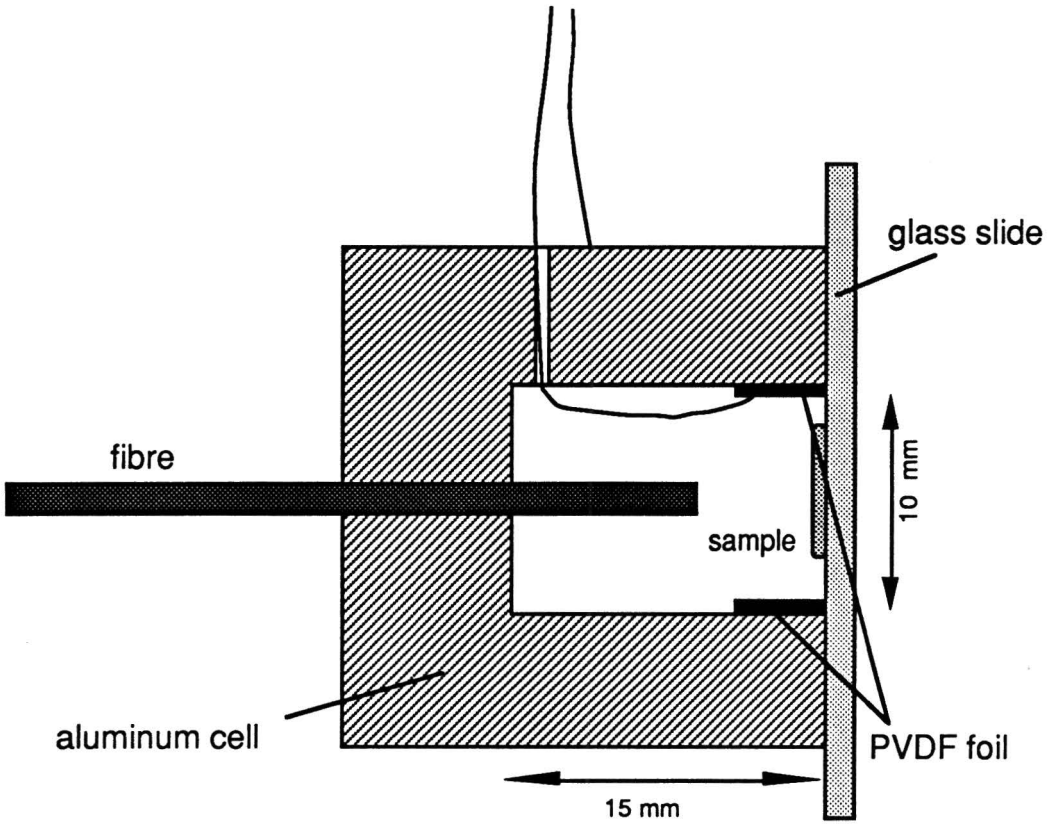

Figure 4.7 First experimental design PA-cell.

The cell is a cylinder made of blank aluminum, because of its low optical absorption, to minimize the self PA-effect of the cell. The samples are fixed on a glass slide, the backing material, which can be removed in order to change the samples easily. The laser light is delivered with a fibre, with a diameter of 600 μm. The fibre is placed far enough from the sample to radiate the sample surface, facing the fibre, completely. As microphone a piece of PVDF, a piezo electric foil, is used. One side of the foil is fixed to the wall of the cell (see figure 4.7) with electric conducting glue to make electric contact with the aluminum. The other side of the foil is connected with a wire that leaves the cell through a narrow channel. This wire together with a wire connected with the outside of the cell provides the signal of the piezo electric foil. Measurements have been carried out with this cell, using samples with controllable absorption: gypsum with an absorber. It appeared that the foil signal increased with decreasing absorption of the sample, which is in contrast with the PA-theory. The

explanation of this effect is that the foil is not only piezo electric but also pyro electric. So it registers, apart from Δp, following the PA-effect, also small temperature changes in the foil due to absorption of the light falling directly or indirectly on it. The amount of reflected or back scattered light increases when absorption of the sample decreases. Two things have been done to get rid of it. A different type of microphone, an electret microphone, is used which is placed at the end of a narrow channel (see figure 4.8) in such a way that light, directly from the fibre or reflected from the sample can not reach the microphone. A second improvement has been made, viz. a cell is used with a smaller radius. This increases the PA-signal, as it is proportional to the reciprocal of the volume of the cell (see equation 4.11). So we end up with a cell as depicted in figure 4.8.

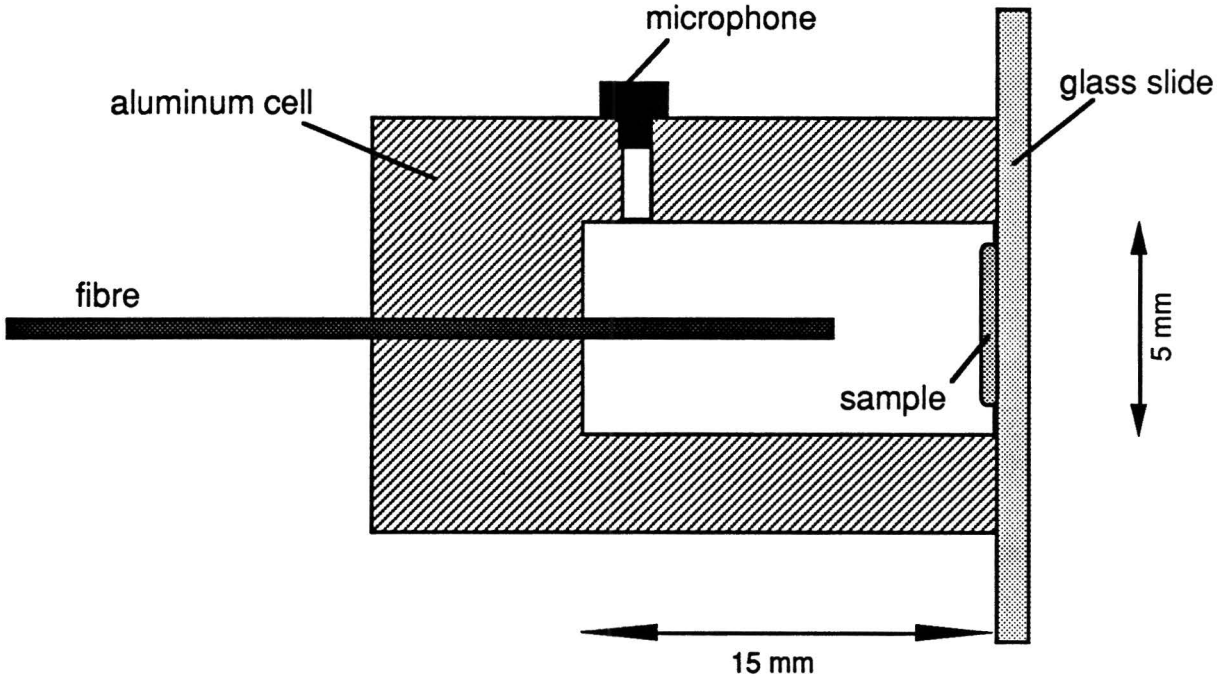

Figure 4.8 Final design of PA-cell.

4.2.3 Experimental set-up

The general set-up of the experiments for obtaining PA-signals is shown below.

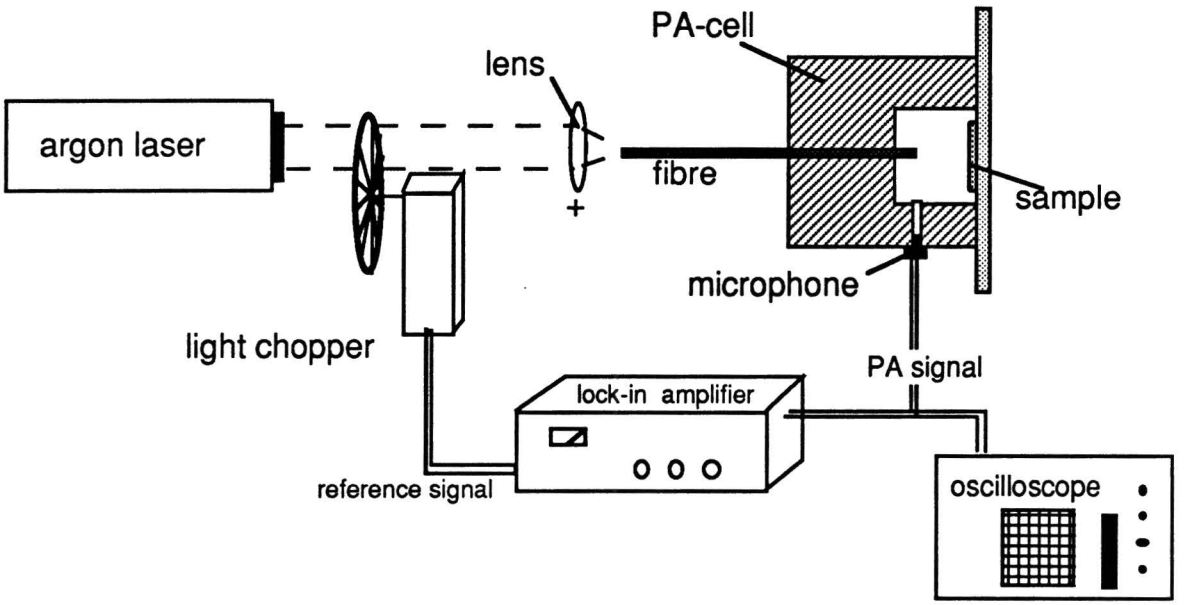

Figure 4.9 General set-up for the PA-measurement.

The exciting light comes from a continuous wave argon laser and is delivered to the PA-cell via a fibre (diameter 600 μm). The argon laser is operated in single line mode, at 501 nm, as this is almost the same wavelength as the wavelength of the pulsed dye laser (504 nm). The samples are pieces of stone, as used in the threshold measurements, glued on a glass slide, the backing material. The sizes of the samples as well as their thermal properties are considered to be the same for all samples. By regulating the chopper frequency care can be taken of the restriction (equation 4.3) that δ_s, the thermal diffusion length should be less than δ_a, the optical absorption length, and l_s, the sample thickness. (To determine δ_s is the aim of these measurements so this restriction can only be verified 'afterwards'.) In that case the PA-signal is proportional to both μ_a and I_0 and not e.g. to thermal or optical properties of the backing material. With the

estimations for the thermal properties of stones in chapter 2 and a chopper frequency of 35 Hz an approximation for δ_s can be obtained:

$$\delta_s \approx 0.1 \text{ mm}$$

which is less than the sample thickness l_s (>2 mm).

The electret microphone, Danavox model 32, converts the PA-pressure signal into an electric signal. This electric signal and a signal from the chopper respectively are the input and reference signal of a lock-in amplifier (see figure 4.9). The electric signal is also visualized on an oscilloscope. The lock-in amplifier gives an output signal proportional to the amplitude of the pressure signal in the cell, when making use of a correction for the frequency response of the microphone (in appendix A).

5. Results

The sequence in which the results of the experiments are presented is the same as used before: first the results of the 'threshold measurements' followed by the results of the 'absorption measurements'.

5.1 Threshold measurements

The measurements to obtain the acoustic threshold energy have been performed with a pulsed dye laser and a pulsed Ho:YSGG laser.

5.1.1 The pulsed dye laser

With the set-up of figure 4.2, and using a pulse energy high enough to create a plasma, the microphone signal due to one laser pulse is displayed in figure 5.1:

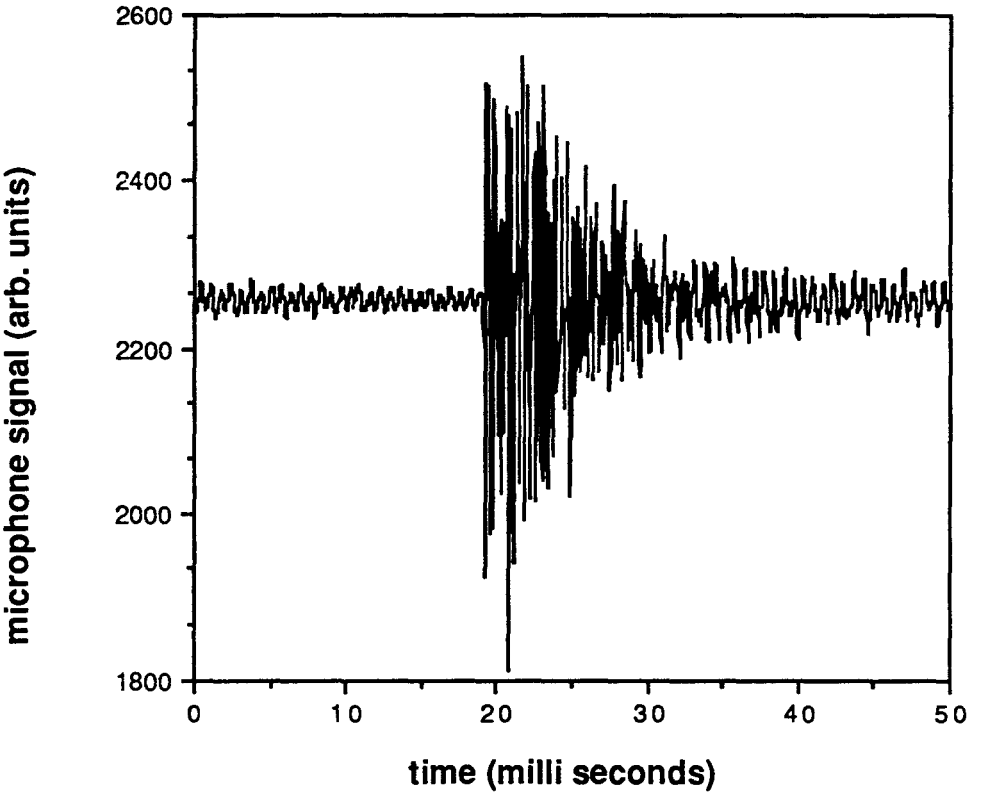

Figure 5.1 Microphone signal of the acoustic wave accompanying a laser pulse

The microphone signal increases almost at the same time as when the laser pulse starts. As the duration of the laser pulse is only 1.5 μs no acoustic effects that occur during the pulse can be observed (the sample frequency is not high enough). Only the shape of the acoustic signal due to one pulse is displayed. It is easy to understand that this is not the signal of the acoustic wave, but the result of resonances in the tank. This effect is assumed to be proportional to the energy of the acoustic wave. The first measurements have been done using aluminum, bakelite and gypsum as samples. Both aluminum and bakelite give reproducible signals and every time a signal is recorded a white flash (plasma) is observed. Gypsum gives very little signals compared with aluminum and bakelite. Also no white flash is observed. On gypsum the effect of these laser pulses seems to be quite different. The results of this experiment is presented in figure 5.2.

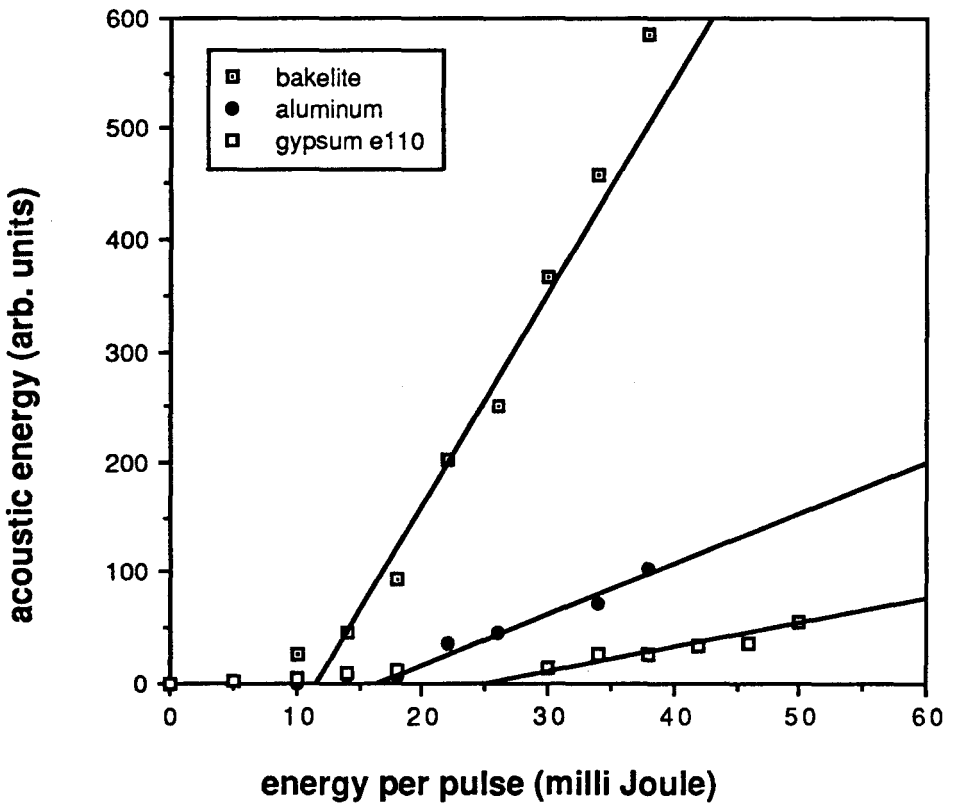

Figure 5.2 Acoustic energy as a function of laser energy for aluminum, bakelite and gypsum.

The laser energy at which the lines cross the horizontal axis are defined to be the threshold energies for acoustic wave generation E_{thr}. In that way the bakelite sample has the lowest threshold energy, $E_{thr} \approx 12$ mJ; for the aluminum sample $E_{thr} \approx 16$ mJ and for the gypsum sample $E_{thr} \approx 25$ mJ. However in the case of gypsum the effect is different and so not comparable to the other samples. When using real stones as samples another problem arises. In contrast with aluminum and bakelite, where not much damage is produced to the surface, much damage is produced to the stone surfaces. This makes the results irreproducible. Results of measurements on gall stones are shown in figure 5.3. It makes this method not suitable to determine E_{thr} for stones: the results of these measurements are not used.

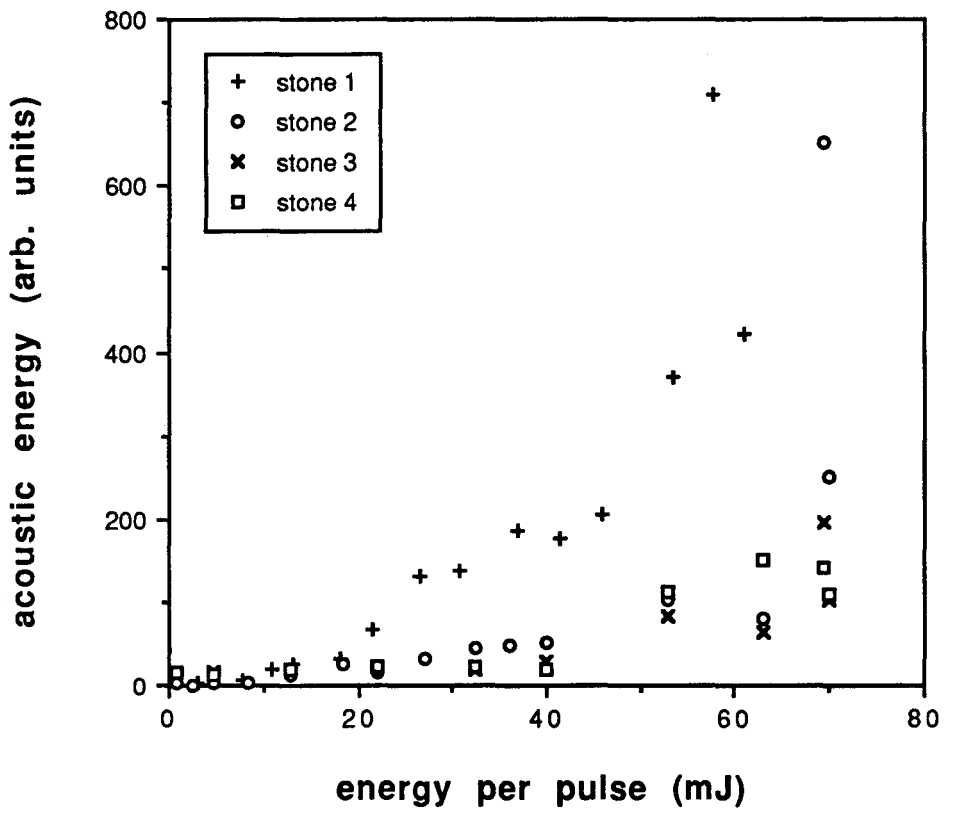

Figure 5.3 Acoustic energy as a function of laser energy for different stones.

For determining the threshold energy for stones, the other method, as described in chapter 4 is used. In order to see if there is any dependence of the threshold energy on the fibre diameter three fibres, with different diameters, are used, namely 200, 400 and 600 μm. The results are presented in two graphs, as the values of the threshold energy in the case of salivary stones is much higher than in the case of gall stones. Figure 5.4 shows the threshold energies for the gall stones and one urinary stone ('bladder') and figure 5.5 for the salivary stones. Some of the gall stones have sides with obviously different optical properties (colour). Such a stone is separated into several samples. E.g. one gall stone had a red and a white side and appeared to be black at the inside; this stone yields three samples: 'gall red', 'gall white' and 'gall black'.

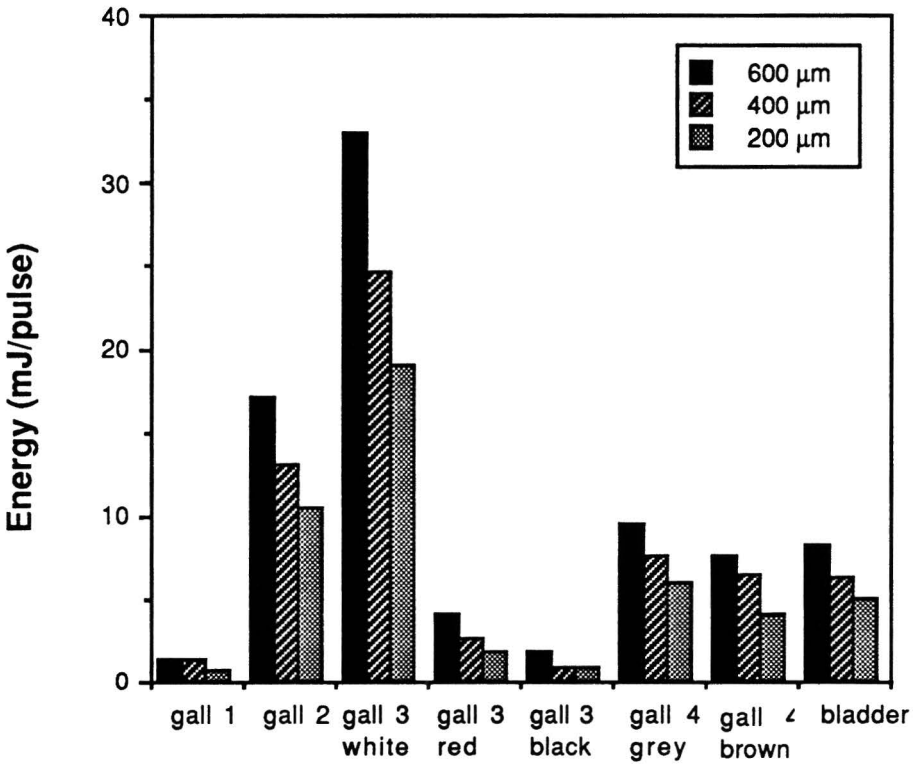

Figure 5.4 Threshold energies of for gall stones.

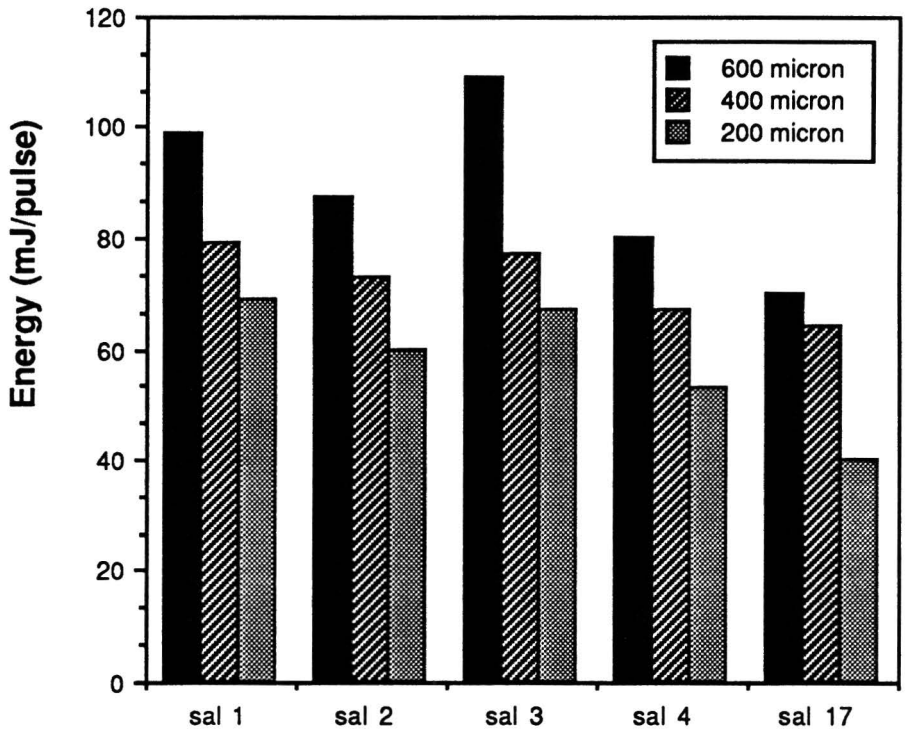

Figure 5.5 Threshold energies for salivary stones.

5.1.2 The pulsed Ho:YSGG laser

With the Ho:YSGG laser similar measurements [16] have been performed as with the pulsed dye laser. The four salivary stones (sal.1 to sal.4) of the previous experiment have been used. Two different fibres were available for use with the Ho:YSGG laser, viz. with a diameter of 320 μm and 600 μm. A remarkable observation was that the acoustic threshold and the plasma threshold were not the same. First acoustic waves are registered and second, with increasing energy, a white plasma flash is observed. The results are listed in the table 5.1.

stone	acoustic threshold (mJ /pulse)		plasma threshold (mJ /pulse)	
	320 μm	600 μm	320 μm	600 μm
sal. 1	75 ± 5	80 ± 5	115 ± 15	440 ± 30
sal. 2	75 ± 5	110 ± 15	100 ± 10	340 ± 25
sal. 3	65 ± 5	125 ± 20	145 ± 15	360 ± 25
sal. 4	70 ± 5	70 ± 10	200 ± 25	440 ± 30

Table 5.1 Threshold energies for different salivary stones, with a pulsed Ho:YSGG laser.

5.2 Absorption measurements

Parts of the stones, for which the threshold energy has been determined, have been investigated photo acoustically. At least one PA-characteristic (amplitude of pressure change, Δp, as a function of intensity of exciting light, I_0) of each stone has been made. If it is easy to see that a stone has sides with different colour, then from each different side a sample has been taken and a PA-characteristic is made (gall red, etc.).

Considering the PA-signal of a sample it is not only the PA-signal of the sample itself, but the PA-signal of the sample and the cell together. This cell PA-signal has been measured by placing no sample on the (glass) slide and it is subtracted from the PA-signal of the samples, in the following way:

$$M_s^2 = M_t^2 - M_b^2 \qquad (5.1)$$

where M_t is the measured microphone (PA) signal of the sample in the cell and M_b is the measured (PA) signal of the cell without sample (background). M_s is the microphone signal due to the sample only. The phase of M_t and M_b is the same. A plot of the PA-characteristic of some samples is displayed in the figure 5.6.

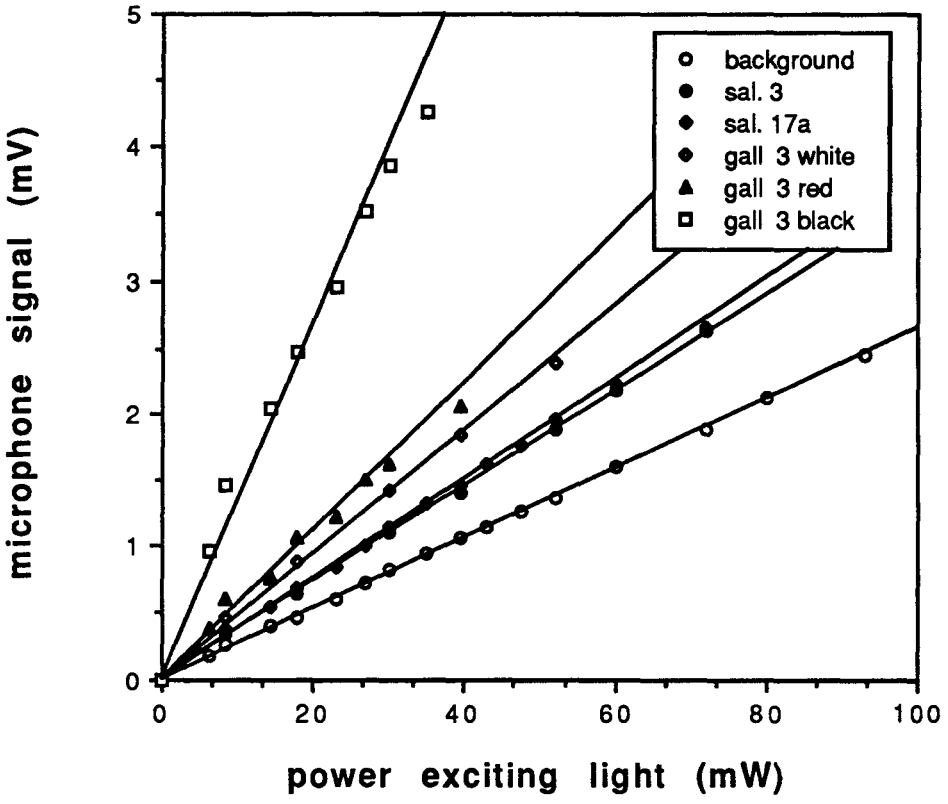

Figure 5.6 PA-characteristics of some samples.

As derived in the previous section the slope of this graph is proportional to the absorption coefficient. Using the geometry of the cell already mentioned, the thermal properties of the samples and the following properties of air [7]:

$$k_g = 0.024 \text{ W/mK}$$
$$c_g = 1000 \text{ J/kgK}$$
$$\rho_g = 1.29 \text{ kg/m}^3$$
$$\gamma = 1.40$$

equation (4.15) becomes a simple linear relation between the ΔP and the power of the exciting light:

$$\Delta p = 0.11\ \mu_a P_0 \qquad (5.2)$$

where I_0 is substituted by P_0, the power of the exciting light. The absorption coefficient is given by the slope of the Δp-P_0 relation. The microphone signal is converted to pressure change by using the microphone frequency response curve (see appendix). The optical absorption coefficients for the samples are calculated and are listed in table 5.2.

stone number	optical absorption coefficient μ_a (mm^{-1})	optical absorption length δ_a (mm)
gall 1	9.5 ± 0.5	0.11 ± 0.005
gall 2	4.6 ± 0.3	0.22 ± 0.013
gall 3 white	4.1 ± 0.3	0.24 ± 0.018
gall 3 red	7.3 ± 0.3	0.14 ± 0.006
gall 3 black	14.6 ± 1.0	0.07 ± 0.005
sal. 1	3.2 ± 0.3	0.31 ± 0.029
sal. 2a	4.3 ± 0.3	0.23 ± 0.016
sal. 2b	3.5 ± 0.3	0.29 ± 0.025
sal. 3	3.1 ± 0.3	0.32 ± 0.031
sal. 4a	3.7 ± 0.3	0.27 ± 0.022
sal. 4b	4.0 ± 0.3	0.25 ± 0.019
sal. 17a	3.2 ± 0.3	0.31 ± 0.029
sal. 17b	4.1 ± 0.3	0.24 ± 0.018

Table 5.2 Results absorption measurements.

Also the absorption length, δ_a, the reciprocal of μ_a, is calculated, to make it easier to verify whether condition (4.3), $\delta_s < \delta_a$, will be fulfilled. At a chopper frequency of 35 Hz δ_s equals 0.1 mm. The measured absorption lengths of the

samples, except one, do satisfy the above condition. Only stone 'gall 3 black' does not, but in this case the experiment is repeated using a chopper frequency of 150 Hz, which makes δ_s equal to 0.047 mm. The value for μ_a is however almost the same (14.6 mm^{-1} at 150 Hz and 14.0 mm^{-1} at 35 Hz).

5.3 Threshold energy versus absorption coefficient

Having obtained the results of the absorption and threshold measurements they can be related to each other (in figure 5.7 on the next page). The optical absorption coefficient for the stones at a wavelength of 2.1 μm (Ho:YSGG laser) has not been measured, but is assumed to be equal to μ_a of water, viz. about 10 mm^{-1} at 2.1 μm. It is clear that the relation, derived in the theory, that $E_{thr} \propto \mu_a$, does not hold, for the different fibre diameters used. Nevertheless we find that E_{thr} increases with increasing μ_a (equation 2.7). A probable explanation for this phenomenon will be given in the next chapter.

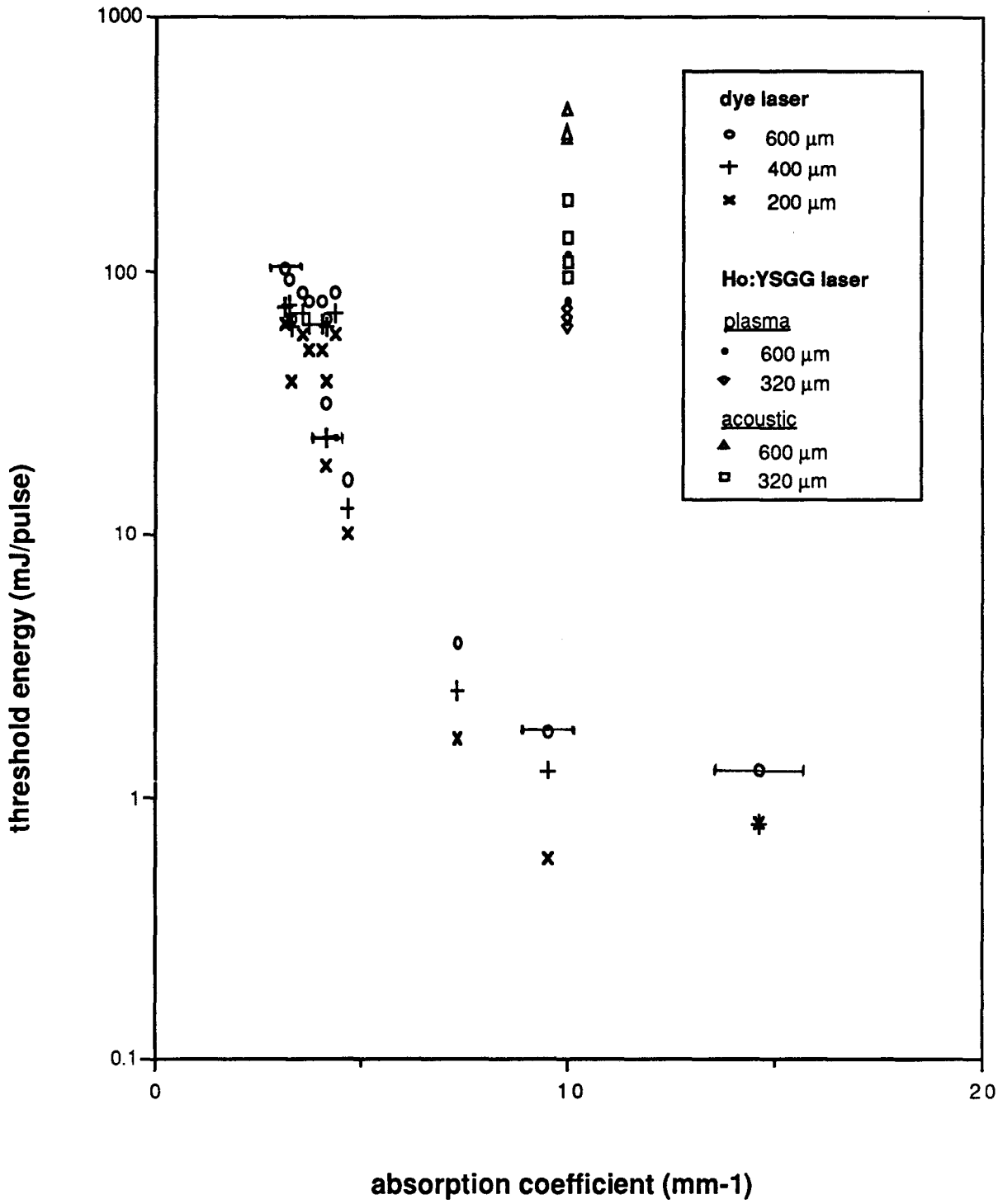

Figure 5.7 Acoustic threshold energy as a function of the optical absorption coefficient, using a different fibre diameters.

6. Discussion

The results will be discussed in relation to the theory from chapter 2. It is easily to see that the results of the experiments do not support the theory. The measured dependence of the threshold energy on both the diameter of the fibre and the absorption coefficient of the sample is different from the theoretical dependence. First the threshold energy in relation to the optical absorption coefficient is discussed, then in relation to the fibre diameter, at last recommendations for further research are given.

6.1 Optical absorption coefficient μ_a

The absorption coefficient obtained for gall stones can be compared with results obtained by Long et al. [17]. They used a different technique, namely pulsed photothermal radiometry. The absorption coefficients they found are between 3.6 mm^{-1} and 16.1 mm^{-1}, thus in the same range as they are obtained with the technique described presently. For salivary stones there are no results to compare with. Figure 5.6 shows that the threshold energy, as defined in chapter 2, depends on the optical absorption coefficient, but not as expected. The μ_a obtained for salivary stones seem to be too high as compared with the μ_a for gall stones. The salivary stones scatter more light back to the walls of the PA-cell than the gall stones do: the PA-signal due to the cell itself (background signal) is not the same for the different stone types. A method should be found to get rid of this background signal or to determine it for each different stone separately.

6.2 Fibre diameter r_f

Looking at figures 5.3 and 5.4 the threshold energy decreases with decreasing fibre diameter, but not as much as it should be following equation (2.7). In the figure below E^*, the threshold energy for the different fibre diameters divided by the threshold energy for a fibre diameter of 600 μm, for some samples is shown. Also the E^* following equation (2.13) is shown.

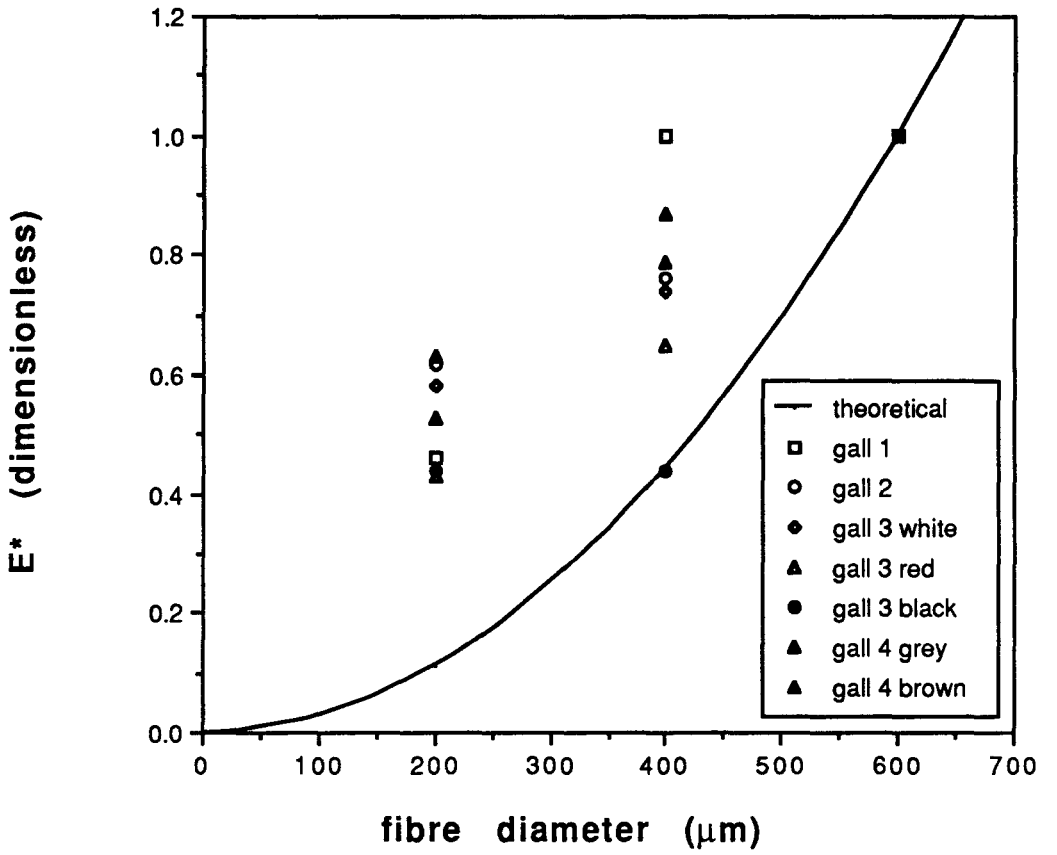

Figure 6.1 The relative E* as a function of r_f.

An explanation for this can not be a heat diffusion process, it has been shown that the time, during which this should take place, is too long compared with the duration of the pulse. If we remember equation (2.7):

$$T_c = \frac{\mu_a}{c_s \rho_s \pi r_{fibre}^2} \int_0^{t_c} P(t)\, dt - T_0 \qquad (2.7)$$

t is replaced by t_c, the time when the dissociation temperature T_c is reached. We assumed that reaching the dissociation temperature T_c is of vital importance for the plasma formation and the fragmentation process. After reaching the dissociation temperature a cloud of dissociated material is formed between

fibre and stone. Before the plasma will be initiated the cloud should be dense enough to be able to absorb enough energy of the laser light needed for ionization. Gas (dissociated material) flowing away between fibre and stone surface will restrict the increase of its density (see figure 6.2):

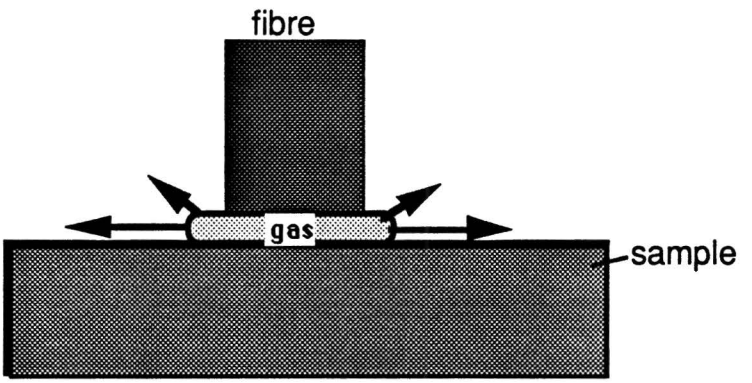

Figure 6.2 Expansion of the cloud of dissociated material between fibre and stone.

Another possible explanation is that the formation of a plasma is not of vital importance for fragmentation, but that the pressure of dissociated material in the cloud should be high enough and build-up fast enough. The absence of the plasma flash above the acoustic threshold, observed with the Ho:YSGG laser, supports this explanation. Consider the pressure build-up not being caused by absorption of laser light by the cloud and subsequent temperature rise, but by a rapid increase of particles, dissociated from the stone surface, into the cloud. The increase takes place during the laser pulse. If after a time t_c a temperature T_c is reached, dissociation of particles starts, following (6.1):

$$\frac{\pi r_f^2}{\mu_a} H_d \frac{\partial n(t)}{\partial t} = P(t) \qquad (6.1)$$

where H_d is the latent heat for dissociation and n(t) is the number of particles produced. Integrating this equation yields:

$$n(t) = \frac{\mu_a}{H_d \pi r_f^2} \int_{t_c}^{t_p} P(t)\, dt \qquad (6.2)$$

The relation between pressure and the amount of particles can be described with the law for ideal gasses. It should be noted that the volume of the cloud increases during the dissociation of the particles (see figure 6.2). The effect of particles flowing to the side of the cloud, causing the volume to increase, is less when using a smaller fibre diameter. Research on the behaviour of the cloud, in particular the pressure inside it, its volume, and the particle flow from the stone to the cloud, e.g with high speed photography, is a recommendation for further research. It is obvious that, if the plasma is not of key importance , the mechanism, proposed in chapter 2 (figure 2.2), does not describe the process properly. A different description of the process is proposed in the figure below:

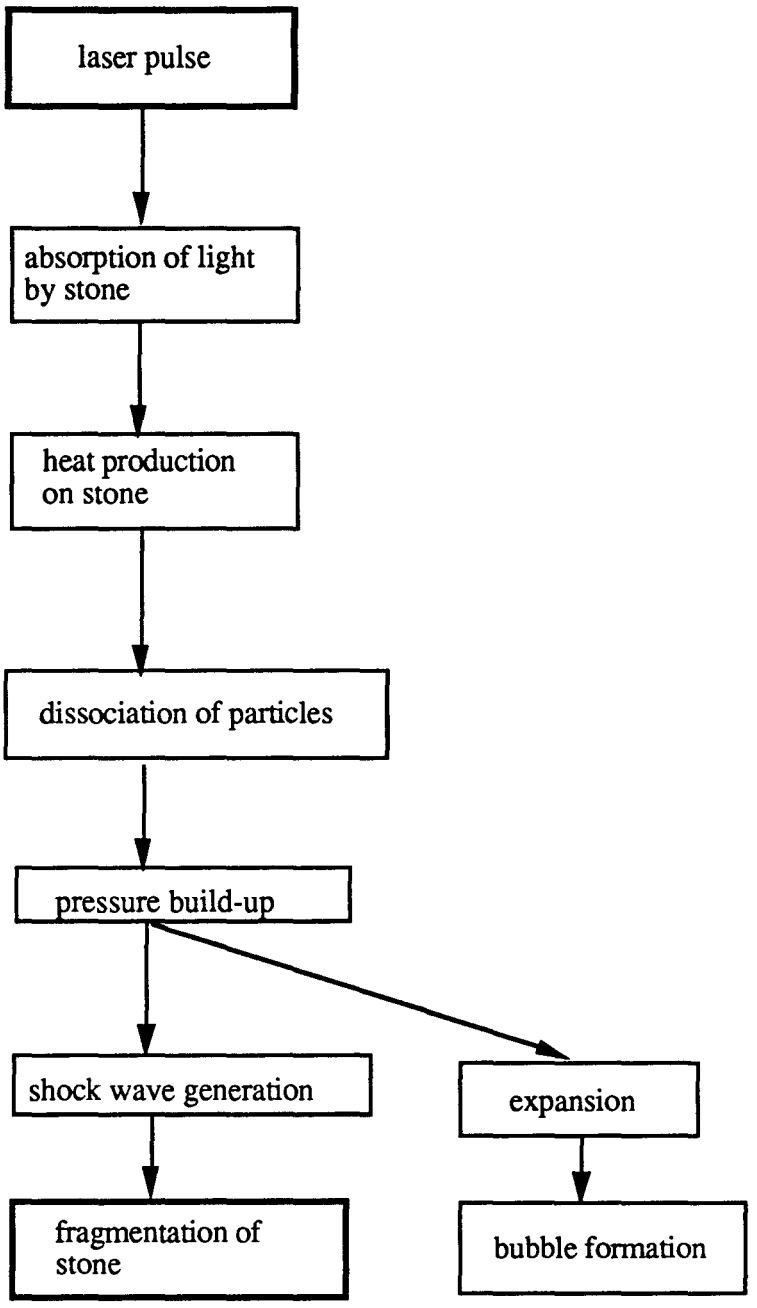

Figure 6.3 New proposed mechanism for describing laser lithotripsy.

Research on the validity of this mechanism is a recommendation for further research.

7. Acknowledgements

At this place I would like to thank everybody, who helped me and cooperated to make this research to a success, and who made me having a (jolly) good time in Amsterdam, especially at the Laser Centre. First of all Dick Sterenborg, my coach at the laser centre, for his indispensable support. Next I want to thank the other people of the Laser Centre, especially Jan Wiersma and my two room mates, David and Johan; Arie Steenbeek, of the mechanical department, for the technical support of the PA measurements; Rens Leeuw of the audiology department, who has been so kind to offer me the possibility of using his audiometry laboratory; Dr. Timmer, of the pharmacology department, who helped me preparing the tablets of hydroxy apatite ('the exploding ones'); Ton van Leeuwen, of the academic hospital in Utrecht, for his help with the experiments using the Ho:YSGG laser; and Dane Bicanic of the physics department of Wageningen University of Agriculture, who taught me the secrets of photo acoustics.

References

[1] M.J.C. van Gemert, W.M. Star: 'Fysische achtergronden van klinisch lasergebruik' edited by M.J.C. van Gemert and T.A. Boon; Samsom Stafleu, Alphen aan den Rijn, Brussels (1987).

[2] G.M. Watson: 'A survey of the action of lasers on stones.; Laser lithotripsy, clinical use and technical aspects' in 'Laser lithotripsy' edited by R. \; Springer verlag, Berlin, Heidelberg, New York, London, Paris. (1988).

[3] J. Cheng, H.J.C.M. Sterenborg, K. Huibregtse: 'Endoscopic laser lithotripsy for large bile duct stones'; submitted to Endoscopy.

[4] P. Teng, N.S. Nishioka, R. Rox Anderson, T.F. Deutsch: 'Optical studies of pulsed-laser fragmentation of biliary calculi'; Applied physics B: 42, 73-78 (1987).

[5] P. Teng, N.S. Nishioka, R. Rox Anderson, T.F. Deutsch: 'Acoustic studies of the role of immersion in plasma mediated laser ablation'; IEEE journal of quantum electronics Q23-10: 1845-1853 (1987).

[6] M.J.C. van Gemert, A.J. Welch: 'Time constants in thermal medicine'; Lasers in surgery and medicine 9: 405-421 (1989).

[7] H.S. Carslaw, J.C. Jäger: 'Conduction of heat in solids'; Clarendon press, Oxford (1986).

[8] J. de Boer, F. Derom, J.A. Gruwez, P.J. Kuijer, G. den Otter, A. Zwaveling: 'Leerboek chirurgie'; Bohn, Scheltema & Holkema; Utrecht, Antwerpen (1985).

[9] L.S. Burstein, A.L. Boskey, P.J. Tannenbaum, A.S. Posner, I.D. Mandel: 'The crystal chemistry of submandibular and parotid salivary glandstones'; Journal of oral pathology, 8: 284-291 (1979).

[10] Soft-500 software system IBM-3, fourth edition; 'Keithley data acquisition & control'; Cleveland (Ohio) (1987).

[11] A.C. Tam: 'Photothermal investigations of solids and fluids, chapter 1'; Academic press; New York San Francisco, London. (1988).

[12] Yoh-Han Pao: 'Opto acoustic spectroscopy and detection'; Academic Press; New York, San Francisco, London. (1977).

[13] A. Rosencwaig, A. Gersho: 'Theory of the photo acoustic effect with solids'; Journal of applied physics, 47: 64-69 (1975).

[14] A.C. Tam: 'Applications of photo acoustic sensing techniques'; Reviews of modern physics, 58:381-425 (1986).

[15] D. Cahen, G. Bults, H.Garty, S. Malkin: 'Photo acoustics in life sciences'; Journal of biochemical and biophysical methods, 3:293-310 (1980).

[16] H.J.C.M. Sterenborg, P.H. van den Akker, F.W. van der Meulen, C.F.P. van Swol, A.G.J.M. van Leeuwen, M.J.C. van Gemert: 'Laser lithotripsy of salivary stones, a comparison between the pulsed dye laser and the Ho:YSGG laser.'; submitted to lasers in medical science.

[17] F.H. Long, N.S. Nishioka, T.F. Deutsch: 'Measurement of the optical and thermal properties of biliary calculi using pulsed photothermal radiometry'; Lasers in surgery and medicine, 7:461-466 (1987)

Appendix

A. Description of electret microphone model 32

The electret microphone, which has been used for the photo acoustic absorption measurement is described. The microphone is a miniature electret condenser microphone, developed for hearing aids, patented in U.S.A. under U.S.A. 4,567,832; patents pending in Europe. It is provided with a hybrid integrated amplifier. The sizes of the microphone are 5.6 mm * 5.6 mm * 2.3 mm (l * w * h). The response (in mV per Pascal) as a function of the frequency has been measured with the following set-up:

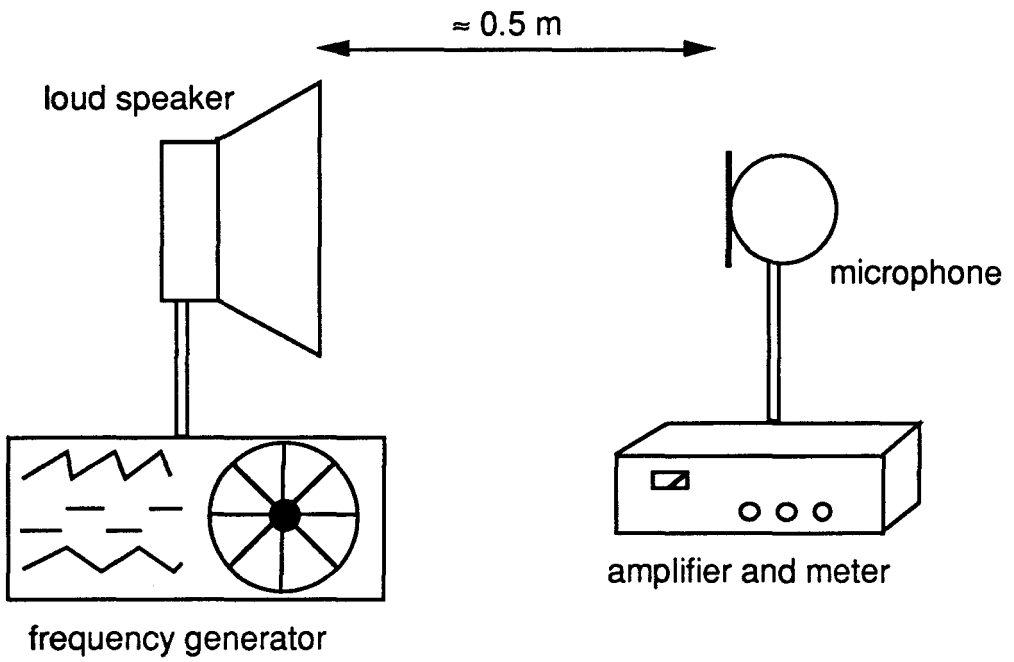

Figure A.1 Experimental set-up to determine the frequency response for a microphone.

The frequency characteristic of the loud speaker has been measured first (in figure A.2), using a calibrated microphone. The response of the 'model 32' microphone as a function of frequency gives a curve as in figure A.3.

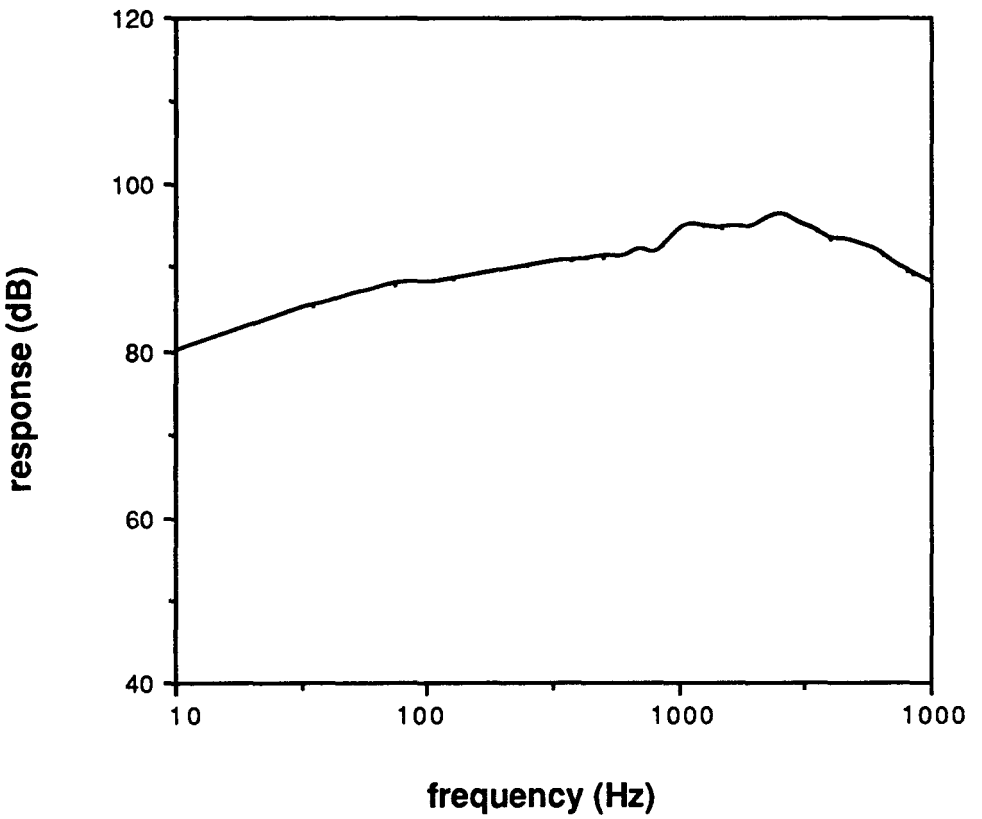

Figure A.2 Response curve for the loudspeaker which is used in the experiments.

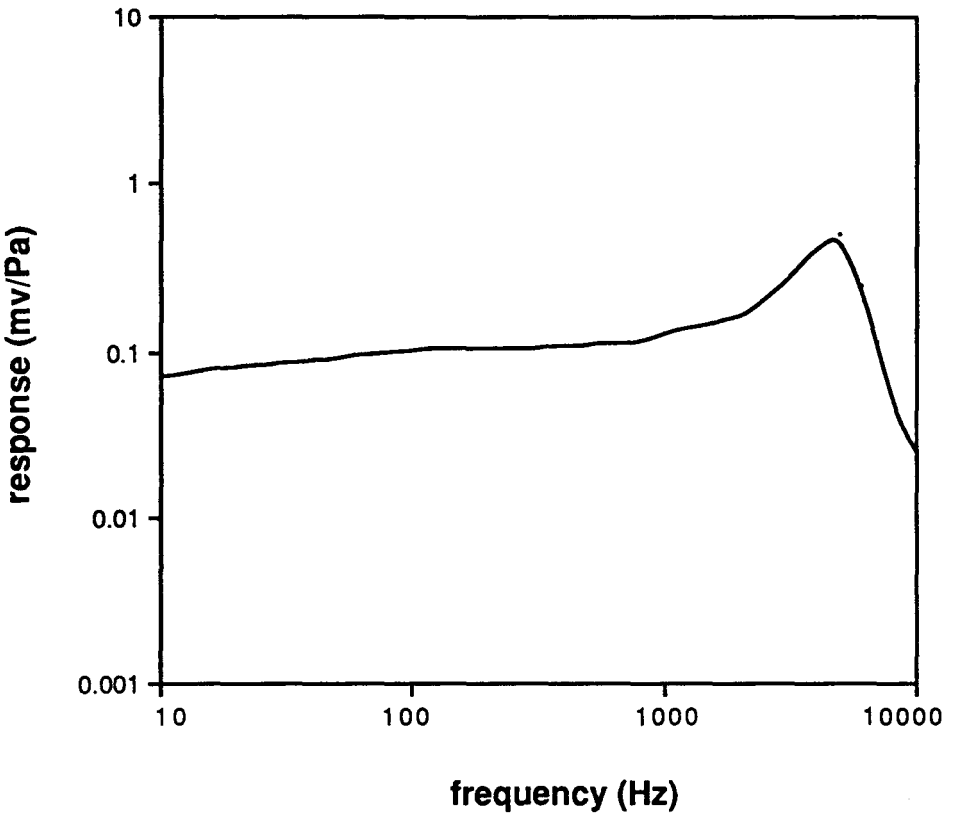

Figure A.3 Typical response curve for the electret condenser microphone ('model 32') which is used in the experiments.

The experiments have been carried out in the audiometry room of the audiology department of the Academic Medical Centre.

B. Results of the measurements

Results of the absorption measurements are displayed in the figures below. They show the microphone signal as a function of the power of the exciting laser light.

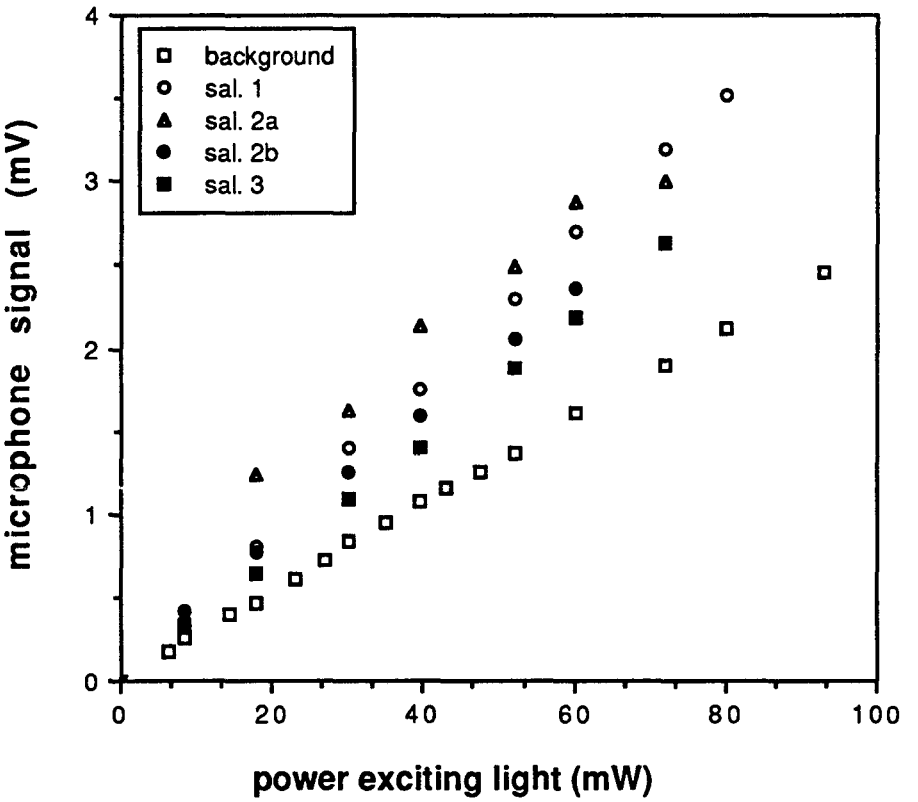

Figure B.1 PA measurements to determine the absorption coefficient of some salivary stones.

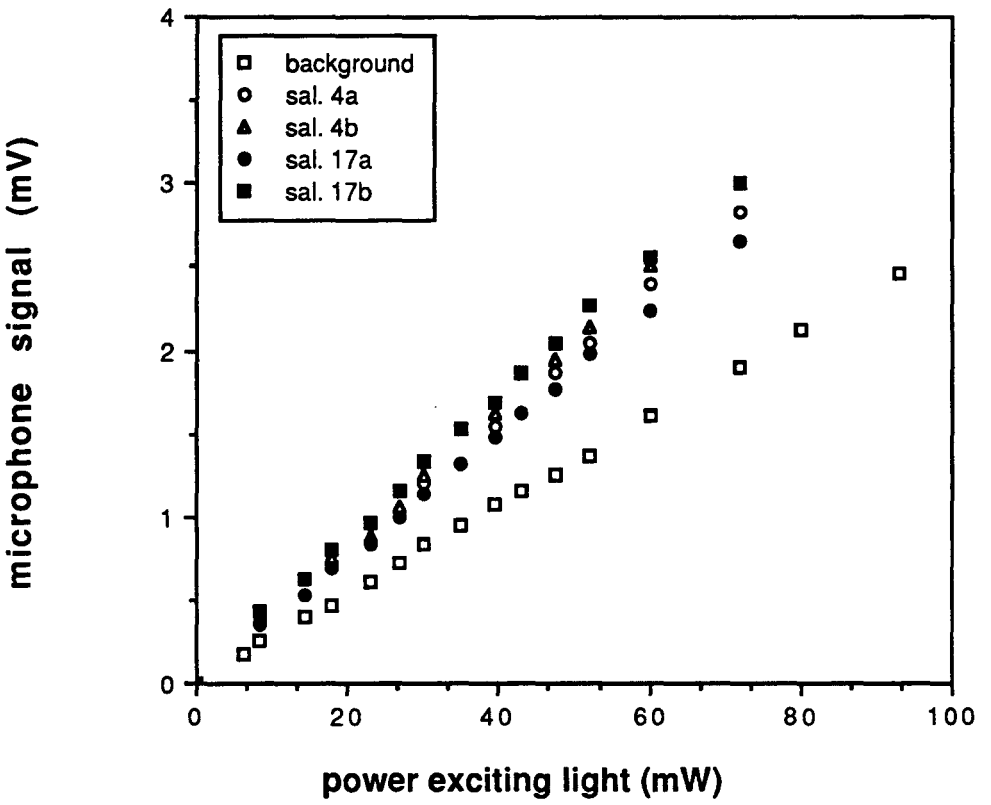

Figure B.2 PA measurements to determine the absorption coefficient of some salivary stones

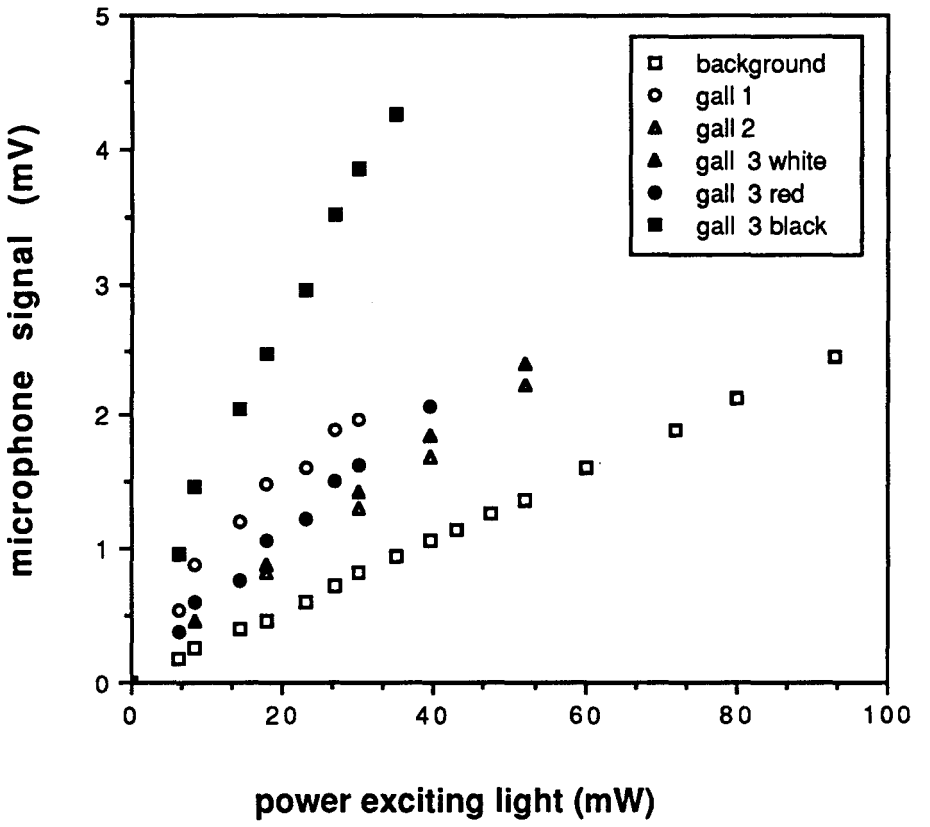

Figure B.3 PA measurements to determine the absorption coefficient of some gall stones; frequency of chopper = 35 Hz.

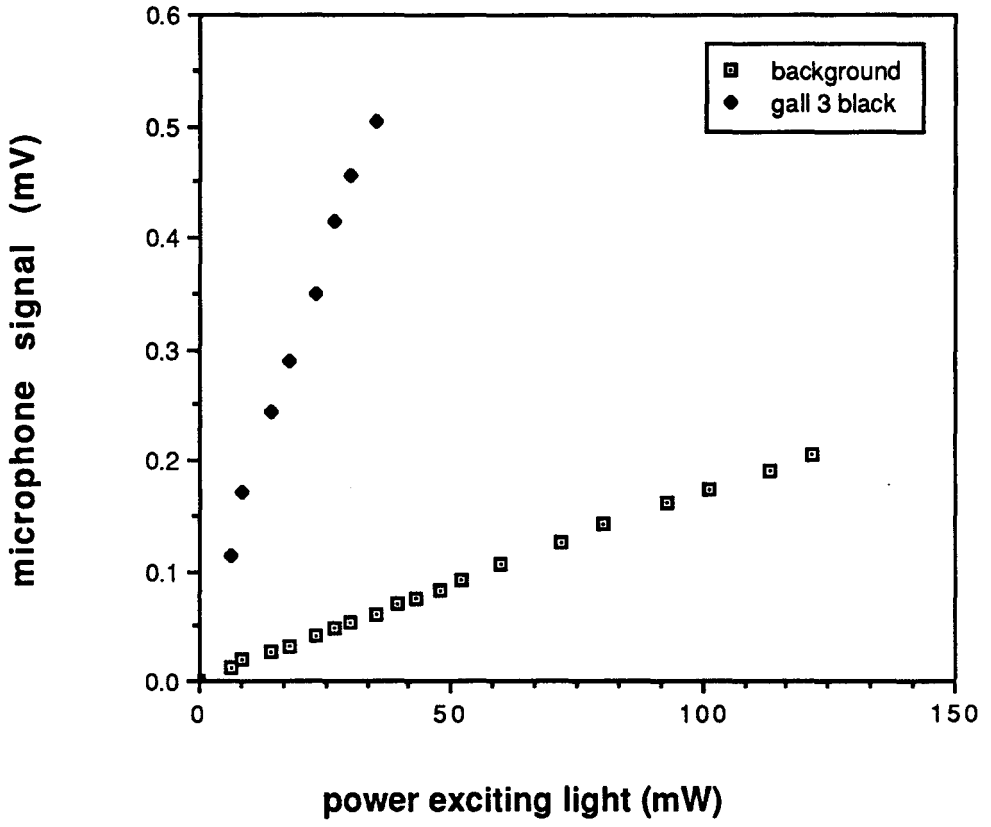

Figure B.4 PA measurements to determine the absorption coefficient of some gall stones; frequency of chopper = 150 Hz.